Recent advances of solid-state nmr spectroscopy for microporous materials

Shenhui Li, Olivier Lafon, Weiyu Wang, Qiang Wang, Xingxing Wang, Yi Li, Jun Xu, Feng Deng

Recent Advances of Solid-state NMR Spectroscopy for Microporous Materials

Shenhui Li, Olivier Lafon, Weiyu Wang, Qiang Wang, Xingxing Wang, Yi Li, Jun Xu*, Feng Deng

Prof. S. H Li, Dr. W.Y. Wang, Prof. Q. Wang, Prof. J. Xu and Prof. F. Deng

National Centre for Magnetic Resonance in Wuhan, State Key Laboratory of Magnetic Resonance and Atomic and Molecular Physics, Key Laboratory of Magnetic Resonance in Biological Systems, Innovation Academy for Precision Measurement Science and Technology, Chinese Academy of Sciences, Wuhan 430071, China.

University of Chinese Academy of Sciences, Beijing 100049, China.

E-mail: xujun@wipm.ac.cn

Prof. J. Xu

Wuhan National Laboratory for Optoelectronics, Huazhong University of Science and Technology, Wuhan 430074, China.

Prof. O. Lafon

Univ. Lille, CNRS, Centrale Lille, Univ. Artois, UMR 8181– UCCS – Unité de Catalyse et Chimie du Solide, F-59000 Lille, France

Institut Universitaire de France, 75231 Paris, France

X. X. Wang, Prof. Y. Li

State Key Laboratory of Inorganic Synthesis and Preparative Chemistry, College of Chemistry, Jilin University, 2699 Qianjin Street, Changchun 130012, China

Prof. Y. Li

International Center of Future Science, Jilin University, Changchun 130012, China

Keywords: porous materials, confined space, structure-property relationship, characterization, solid-state NMR

Abstract

Microporous materials has attracted a rapid growth of research interest in materials science and multidisciplinary area because of their wide applications in catalysis, separation, ion exchange, gas storage, drug release and sensing. A fundamental understanding of their diverse structures and properties is crucial for rational design of high-performance materials and technological applications in industries. Solid-state NMR (SSNMR) capable of providing atomic-level information on both structure and dynamics is a powerful tool in the scientific exploration of solid materials. In this contribution, advanced SSNMR instruments and methods for characterization of microporous materials is briefly described. The recent progresses of the application of SSNMR in the investigation of microporous materials including zeolites, metal-organic frameworks (MOFs), covalent-organic frameworks (COFs), porous aromatic frameworks (PAFs) and layered materials are discussed with representative work. The versatile SSNMR techniques provide detailed information on the local structure, dynamics, and chemical process in confined space of porous materials. The challenges and prospects in SSNMR study of microporous and related materials are discussed.

1. Introduction

Porous materials are of great interest from both fundmental and technological perspectives. Amongst various types of porous materials, microporous materials (with pore diameter < 2 nm), such as zeolites, metal-organic frameworks (MOFs), covalent-organic frameworks (COFs), and porous aromatic frameworks (PAFs), combine high specific surface areas, large pore volumes and shape-selectivity effects, which makes them key materials for a wide range of applications, including catalysis, gas separation/purfication, ion exchange, gas storage, and sensing.

The diverse framework compositions and functionalities of microporous materials represent a huge challenge for their structural characterization as well as evaluation of their performances. Analytic tools such as X-ray diffraction (XRD), electron microscopy and adsorption-desorption isotherms are now routinely employed for characterization of microporous materials in order to establish the structure-property relationships, and hence, to facilitate the rational design of advanced materials with improved property. However, the structure determination of porous materials using single crystal XRD requires the high crystalline and long-range ordering of the framework. Solid-state NMR (SSNMR) has emerged as a powerful spectroscopic technique with atomic-level resolution, complementary to XRD, in the investigation of structures in materials science due to its sensitivity to geometries and orderings in short to medium range. [1] Information on the chemical composition, local environment, pore connectivity, and coordination network of porous materials can be retrieved from a variety of NMR parameters. Besides, SSNMR is able to provide detailed information on dynamic behavior of molecules at different time scales and probe host-guest interactions.

Tremendous progress has been made in the field of SSNMR study of microporous materials in the past decades.[1c, 2] Multinuclear and multidimensional SSNMR techniques have been extensively utilized to characterize the framework structure of porous materials and explore

the dynamics of guest molecules. The self-diffusion coefficient and diffusion pathway of guest molecules along the channels of porous materials have be examined by pulsed field gradient (PFG) NMR spectroscopy. Hyperpolarized ^{129}Xe NMR can be employed to investigate the cage and channel structure and the communication in porous materials. [3] Variable temperature (VT) SSNMR is a well-established tool for elucidating the molecular flexibility and dynamic behavior of porous functional materials. [4] SSNMR exhibits great potential for investigating the host-guest interaction between small molecules and porous materials. [2c, 5] Furthermore, in situ SSNMR is becoming increasingly important in the study of catalytic reaction mechanism over microporous materials by observing reactive intermediates trapped in voids or channels. Instrumentation and techniques have been recently developed to improve the sensitivity of SSNMR of materials and detect the signal of nuclei of interests with low natural abundance, small gyromagnetic ratio (γ), or subject to large quadrupole interactions.

In this report, novel SSNMR methods and advanced instruments utilized to characterize microporous materials are briefly introduced. Recent advances in the application of SSNMR in porous materials are critically reviewed with focus on the progress on zeolites, MOFs, COFs, PAFs, and layered materials. We discuss how the scientific issues relevant to the structures, interactions and dynamics involved in these fascinating porous materials can be addressed by advanced SSNMR spectroscopy. The challenges and prospects of SSNMR techniques for the study of porous materials are also described.

2. Brief introduction of SSNMR methods and instruments

2.1 NMR parameters and relation with structural information for materials

SSNMR is an element-specific method, which provides a high content of information on solid materials. SSNMR spectra feature signal broadening as compared to the high resolution signals of solution-state NMR, owing to various anisotropic interactions in materials without

sufficient molecular motion, including dipolar interaction, chemical shift anisotropy (CSA), and quadrupolar interaction for quadrupolar spin with $I \geq 1$. Since these interactions are highly sensitive to the chemical and electronic environment, local geometry and dynamic behavior, they can be used to extract important information on the structure and chemical process. For example, adsorbed CO_2 in MOFs exhibits restricted molecular motion due to the strong interaction between CO_2 and metal center, which results in an evident CSA powder pattern in the ^{13}C NMR spectra.[6] The CSA can be determined through spectral fitting of one-dimensional (1D) static spectral pattern or magic angle spinning (MAS) sidebands, as well as extracted from two-dimensional (2D) NMR experiments refocusing CSA in indirect dimension. For quadrupolar nuclei with half integer spin, such as the framework element ^{27}Al ($I = 5/2$) in zeolite and metal ion ^{25}Mg ($I = 5/2$) in MOFs, 2D multiple quantum (MQ) MAS NMR technique[7] allows achieving high-resolution isotropic spectra after eliminating second-order quadrupolar interaction by which the framework site with different coordination numbers can be differentiated. Quadrupolar coupling constant (QCC) and asymmetry parameter η can be extracted from the MQMAS NMR spectra to provide refined information on the geometry of the structural unit with similar coordination state. An example is the identification of distorted tetrahedral Al in mordenite zeolite by its larger QCC from ^{27}Al triple-quantum (3Q) MAS NMR measurement.[8]

The isotropic chemical shift (δ_{iso}) in high-resolution spectra provides a straightforward and simple way to get structural information for porous materials, such as ^{29}Si NMR for zeolites, ^1H and ^{13}C NMR for MOFs, COFs and PAFs. Dipolar decoupling is often required to obtain a high-resolution spectra of these nuclei by removing or reducing the broadening effect due to the dipolar couplings. On the other hand, the dipolar couplings, which depend on the internuclear distance, are very useful for extracting valuable information on connectivities and proximities between the same or distinct nuclei. Proximities between ^{29}Si nuclei in zeolites can be probed through ^{29}Si-^{29}Si dipolar couplings (through-space), which can be reintroduced

under MAS by application of recoupling schemes. This recoupling has been incorporated into 2D double-quantum-single-quantum (DQ-SQ) homonuclear correlation experiment, which gives information on the $^{29}Si-O-^{29}Si$ proximities, as well as internuclear distances.[9] The proximities between protons in zeolites and MOFs have also been observed using 2D through-space SQ-SQ or DQ-SQ homonuclear correlation experiments through dipolar recoupling.[10] DQ-SQ experiment allows the observation of the proximities between the sites with close δ_{iso} values. Additionally, $^{29}Si-O-^{29}Si$ J-couplings (through-bond) have been used to identify the ^{29}Si sites linked by Si-O-Si bridge in zeolites.[11] This connectivity information has notably been obtained at natural abundance using 2D ^{29}Si refocused incredible natural abundance double-quantum transfer experiment (INADEQUATE). Information on the proximities between half-integer spin quadrupolar nuclei with $I \geq 3/2$, such as ^{27}Al, can also been obtained using 2D through-space DQ-SQ homonuclear correlation experiments.[12] For example, detailed spatial correlations among various aluminum species in dealuminated HY zeolite were revealed by ^{27}Al DQ-MAS NMR spectroscopy.[12a]

Spatial connectivities and proximities between two distinct nuclei can be probed using 2D heteronuclear correlation (HETCOR) experiment. The polarization transfer could be established through-bond correlation using heteronuclear multiple-quantum coherence (J-HMQC) or through-space correlation utilizing cross polarization (CP) or heteronuclear multiple-quantum coherence (D-HMQC) experiments. For example, the $^{11}B-O-^{29}Si$ and $^{29}Si-O-^{27}Al$ connectivities in zeolites have been probed using J-HMQC experiments.[13] Internuclear distances can be quantitatively determined by rotational-echo double-resonance (REDOR)[14] when the dephaser isotope has a spin $I = 1/2$, or its variants including transfer of population in double-resonance (TRAPDOR)[15] and the rotational-echo adiabatic-passage double-resonance (REAPDOR)[16] suitable for quadrupolar dephaser isotope. More recently, rotational-echo saturation-pulse double-resonance (RESPDOR) sequence has been introduced as an alternative to REAPDOR and TRAPDOR methods.[17] Compared to TRAPDOR and

REAPDOR, RESPDOR experiment requiring moderate radio frequency (RF) field is compatible with high speed MAS, and for an isolated spin pair, its dipolar dephasing can be expressed by an analytical formula, which allows a rapid determination of internuclear distances. The host-guest interactions and Al–C proximities in dealuminated HY zeolite[17b] and in MIL-100(Al) framework[18] were explored using ^{27}Al–^{13}C S-RESPDOR NMR experiments.

2.2. Sensitivity enhancement technique

A major limitation of solid-state NMR spectroscopy is its relatively low sensitivity owing to the small nuclear magnetic moments. The low sensitivity impairs the observation of diluted species or insensitive isotopes with low γ, such as ^{67}Zn and ^{91}Zr, or low natural abundance, such as ^{15}N and ^{17}O. Besides the isotope enrichments strategy, advanced SSNMR instruments and methods can effectively enhance NMR detection sensitivity. One approach to increase the sensitivity is to use high static magnetic fields, B_0. Higher fields bring gains of sensitivity roughly proportional to $B_0^{7/4}$ for spin-1/2 isotope and $B_0^{11/4}$ for half-integer quadrupolar nuclei. Higher fields also improve the resolution, which is proportional to B_0 and B_0^2 for spectral dimensions corresponding to spin-1/2 and half-integer quadrupolar nuclei, respectively. Thanks to the availability of high-field (> 18.8 T) NMR spectrometers, the NMR spectra with significantly enhanced spectral resolution were recently reported for half-integer quadrupolar nuclei in microporous materials such as ^{27}Al in zeolite,[19] ^{25}Mg and ^{67}Zn in MOFs.[20] Further gain in sensitivity can be obtained using Carr-Purcell Meiboom-Gill (CPMG) detection or its QCPMG variants for quadrupolar nuclei.[21] In recent years, dynamic nuclear polarization (DNP) has also been demonstrated a promising technique to enhance the NMR signal of microporous materials.[22] This technique utilizes the microwave-driven transfer of polarization from unpaired electrons to the nuclear spins and yields sensitivity gain by one to three orders of magnitude. The DNP-NMR system generally includes a high-power

microwave source, such as a gyrotron, and a cryogenic MAS probe, which operates at temperature of 100 K. Furthermore, MAS DNP experiments at $B_0 \geq 5$ T generally requires the introduction of nitroxide biradicals into the investigated materials, which act as the source of polarization. The sensitivity gain provided by DNP has enabled the detection of insensitive isotopes, such as ^{15}N, [119]Sn and [195]Pt,[22-23] as well as diluted species.[24]

3. SSNMR characterization of zeolites

Zeolites are inorganic crystallites containing pores of molecular dimensions and cavities with well-defined structures and are widely applied in diverse areas such as catalysis, ion exchange, and separations in chemical and petrochemical industry. The three-dimensional four-connected framework of classical aluminosilicate zeolite, made up of corner-sharing TO_4 (T = Si and Al) tetrahedra, can be comprehensively characterized by the well-established NMR experiments. Advanced SSNMR techniques afford detailed information on the framework or extra-framework species, host-guest interactions and catalytic reactions occurring in the confined space of zeolites.

3.1 Characterization of zeolite framework

Multidimensional and multinuclear (^{29}Si, ^{27}Al, [17]O) SSNMR have been extensively applied in the structural characterization of zeolites. ^{29}Si NMR chemical shifts are very sensitive to the local chemical environments of framework.[25] The topology structure of purely siliceous zeolite could be determined by a combination of ^{29}Si DQ MAS NMR spectroscopy and powder XRD, which relies on the framework's crystallinity and spectral resolution of ^{29}Si NMR. The [29]Si–[29]Si distances of different Si pairs within framework can be elucidated from the [29]Si DQ build-up curves as a function of homo-nuclear recoupling times.[9a, b] Moreover, the [29]Si–O–[29]Si scalar couplings[11] and CSA[26] of pure silicon zeolite extracted from 2D refocused-INADEQUATE ^{29}Si{^{29}Si} NMR and 2D CSA recoupling NMR experiments could serve as structural constrains for solving the 3D framework structure. The [29]Si–O–[29]Si

connectivities within the as-synthesized zeolites ITW and MTT were established through 2D ^{29}Si{^{29}Si} DQ MAS NMR experiments, which shed light on complicated order and disorder within their frameworks.[27]

Smeets and coworkers applied DNP-enhanced 2D ^{29}Si homo- and hetero-nuclear correlation NMR to establish the through-bond connectivities of distinct Si sites and investigated the local structure of calcined Si-SSZ-70 at natural ^{29}Si isotopic abundance (4.7%).[28] **Figure 1a** shows 1D ^{29}Si MAS NMR spectrum of calcined Si-SSZ-70, which consisted of Q^4 sites (−105~−121 ppm) and Q^3 sites (−95~−104 ppm). In the DNP-enhanced 2D ^{29}Si{^{1}H} HETCOR spectrum (Figure 1b), ^{29}Si signal at −99 ppm from interlayer Q^3 silanol species was spatially correlated with the ^{1}H signal at 3.0 ppm from isolated silanol groups. Additionally, the ^{29}Si signal at −99 ppm was correlated with the ^{1}H signal at 8.8 ppm arising from the strongly H-bonded −SiOH moieties. The covalent ^{29}Si−O−^{29}Si connectivities of nearest neighbor Q^3 and Q^4 sites were clearly manifested from the DNP-enhanced 2D ^{29}Si{^{29}Si} J-mediated correlation spectrum (Figure 1c). As indicated in blue lines, the Q^4 Si2b signals were correlated with the peaks at ca. −112 ppm from Si4b and Si3 sites, which were spatially connected with the signals at ca. −116 ppm from Si5b and Si6 sites. The 2D ^{29}Si{^{29}Si} J-mediated correlation spectrum exhibited the covalent linkages Si1b−O−Si2b−O−Si4b−O−Si5b and Si1b−O−Si2b−O−Si3−O−Si6 (blue lines), confirming the proposed model 1 (Figure 1d). Similarly, the Si−O−Si covalent interconnectivities between the Q^3 Si2b silanol moieties and Q^4 sites at the intralayer channel surfaces (Si2b−O−Si4b−O−Si5b and Si2b−O−Si3−O−Si6) were clearly observed in red lines, corresponding to the proposed model 2 (Figure 1d). Further DFT calculations would be helpful to support the assignments of various Si sites. The high sensitivity of the 2D DNP-enhanced ^{29}Si NMR spectra provided direct evidence for the presence of two distinct types of Q^3 silanol species and their detailed bonding environments at local atomic-level connectivity in the partially disordered system (Figure 1e).
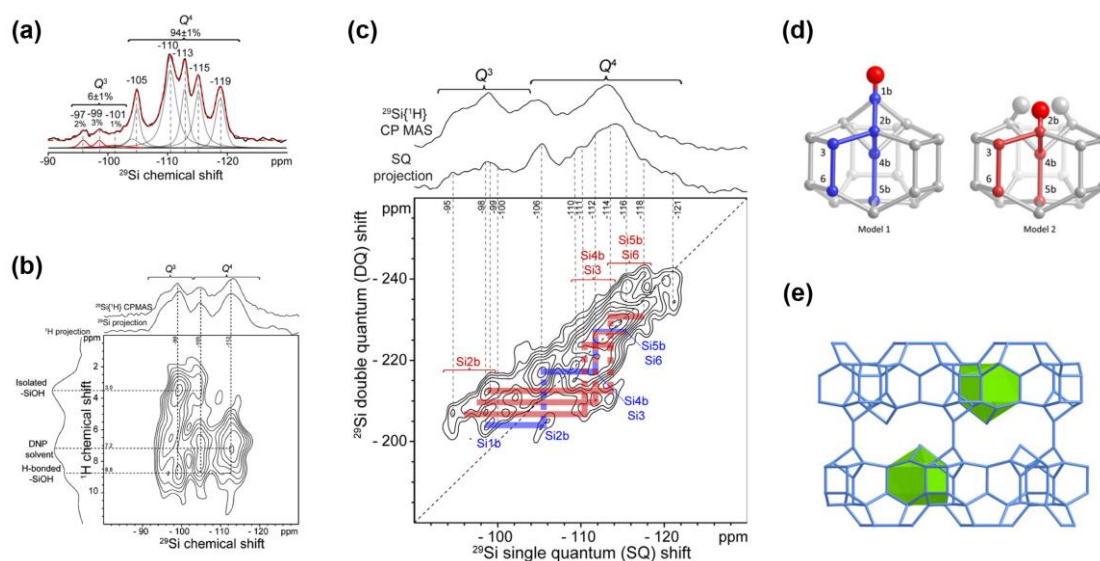
9

Figure 1. (a) 1D ^{29}Si MAS NMR spectrum, (b) DNP-enhanced 2D ^{29}Si{^{1}H} dipolar-mediated HETCOR spectrum and (c) DNP-enhanced 2D ^{29}Si{^{29}Si} *J*-mediated correlation spectrum of calcined Si-SSZ-70. (d) Cage structure for model 1 showing the four-site connectivity path with blue lines and for model 2 showing the three-site connectivity path with red lines. (e) Structural illustration of the interlayer region of calcined Si-SSZ-70. Reproduced with permission.[28] Copyright 2017, American Chemical Society.

The framework of doubly ^{29}Si- and ^{17}O- isotopically enriched Ge-UTL derived from assembly, disassembly, organization, reassembly (ADOR) method was fully examined by ^{29}Si and ^{17}O MAS NMR to monitor the hydrolysis and rearrangement process.[29] The ^{29}Si and ^{17}O NMR experiments reavelaed that the hydrolysis and rearrangement process proceeded over a much longer time scale than observed by XRD. To understand how the neutral liquid water affects the stability of the zeolite framework under mild conditions, Christopher and coworkers found that the covalent bonds in zeolite chabazite (CHA) underwent partial hydrolysis in contact with neutral liquid water at mild condition by using ^{27}Al, ^{29}Si and ^{17}O MAS NMR.[30] This process was fully reversible without framework degradation. ^{17}O MAS NMR was also used to obtian detailed structural information on the surface oxygen sites [31] and framework linkages

10

[32] in zeolites and related materials. A quantitative analysis of the distribution and sitting of aluminum for different T-sites in H-BEA zeolite was achieved by using ^{27}Al MAS NMR in combination of extended X-ray absorption fine structure (EXAFS) spectroscopy.[33] Different Al distributions were observed in zeolite with the same framework topology. Tri-coordinated framework Al acting as Lewis acid sites was identified by using advanced NMR methods including ^{27}Al{^{1}H} REDOR MQMAS NMR, ^{31}P{^{27}Al} through-space HMQC and ^{31}P{^{27}Al} S-RESPDOR MAS NMR experiments.[34]

Undertanding of synthesis mechainsm is essential for guding a rational design of robust materials. ^{27}Al, ^{29}Si, and ^{31}P SSNMR have been used as probes to monitor the crystallization of framework and examine intermediate phases in the synthesis of Beta and ZSM-5,[35] silicalite-1[36] and microporous aluminophosphate molecular sieves such as SAPO-34[37] and AlPO$_4$-5[38]. The evolution and rearrangment of the primary structure units composed of Si, Al or P atoms from the amorphous phase to crystalline framework as revealed by multinuclear SSNMR provied detailed insights into the crytallizaiton mechanisms of these microporous materials of industrial interest.

Sn(IV) isomorphously substituted into Sn-β zeolite represents a breakthrough in the exploitation of atom-efficient solid Lewis acid catalysts because of its unparalleled catalytic performance in biomass conversion. The characterization of framework Sn site is a subject of intensive studies. The so-called open (e.g. (SiO)$_3$Sn-OH) and closed (e.g. (SiO)$_4$Sn) Sn sites were proposed. Dynamic Nuclear Polarization Surface-Enhanced NMR Spectroscopy (DNP-SENS) technique[22] was recently applied on Sn-β zeolites. On the basis of ^{119}Sn chemical shifts, closed and open Sn sites were differentiated in Sn-β prepared with postsynthetic and hydrothermal method. Recently, two types of open Sn sites containing Sn-OH groups were selectively observed by proton-detected 1D and 2D ^{1}H{^{119}Sn} dipolar-mediated *D*-HMQC NMR spectroscopy.[39] The concentration of these open site was determined to be to ca. 17 %

of the total Sn atoms in framework. Furthermore, 2D ^{1}H{^{29}Si} D-HMQC NMR experiment revealed a reversible transformation between the open and closed Sn sites.

3.2 Characterization of extra-framework species in zeolites

Apart from zeolite framework, there is an increasing of interest in the study of extra-framework metal species in zeolites. The introduction of metals (Zn, Ga, Mo, etc.) or metal oxides into zeolites results in bifunctional catalysts of combined acidity and redox property, considerably enhancing their catalytic performances compared to unmodified ones. The property and catalytic performance of metal-modified zeolites depends on the metal speciation, distribution and interactions on zeolites.

SSNMR investigation of metals of interest, such as ^{67}Zn and ^{95}Mo, is very challenging due to their very low γ and low natural abundance, and large quadrupolar moment as well as the low metal loading (few wt% of the sample) in zeolite like Zn/ZSM-5 and Mo/ZSM-5. In order to tackle these challenges, it is always necessary to combine isotopic enrichments during sample preparation, ultra-high magnetic field spectrometer, and advanced pulse sequences to enable the NMR detection. Ultra-high field ^{95}Mo NMR (21.1 T) was employed to investigate the introduced Mo species on ^{95}Mo isotopically enriched-ZSM-5, which showed that the ion-exchanged Mo species was active center for methane dehydroaromatization reaction.[40]

Qi and coworkers applied ^{67}Zn and ^{1}H{^{67}Zn} double-resonance MAS NMR to detect the surface Zn species and their spatial interaction with Brønsted acid sites on Zn-modified ZSM-5 zeolite.[21b] A sensitivity-enhanced hyperbolic secant (HS) and Quadrupolar Carr−Purcell−Meiboom−Gill (QCPMG) NMR technique combined with at high magnetic field (18.8 T) produced a 16-fold ^{67}Zn NMR signal enhancement on natural abundance ZnO powder and allowed structural characterization of the ^{67}Zn isotope-enriched ZSM-5 samples (Zn/H-ZSM-5). As shown in **Figure 2a**, ^{67}Zn HS-QCPMG NMR spectra of Zn/H-ZSM-5 exhibited two ^{67}Zn signals with isotropic chemical shifts of 224 and 238 ppm, ascribed to

12

Zn^{2+} ions located on the cation exchange sites of ZSM-5 and highly dispersed ZnO particles respectively. The ^{1}H{^{67}Zn} S-RESPDOR NMR spectra offered direct experimental evidence on the spatial proximity between Brønsted acidic protons and zinc species as reflected from the significant signal dephasing for the SiOHAl (at 4.3 ppm) [41] (Figure 2b). The ^{1}H–^{67}Zn internuclear (2.70~3.34 Å) distance between the Brønsted acidic proton and zinc atom was determined by the S-RESPDOR experiment (Figure 2c). The spatial interaction between Zn^{2+} ion and Brønsted acid site lead to the formation of synergic active site on Zn/H-ZSM-5, which induced an enhanced Brønsted acid strength and activity for C–H bond activation of methane.[21b]
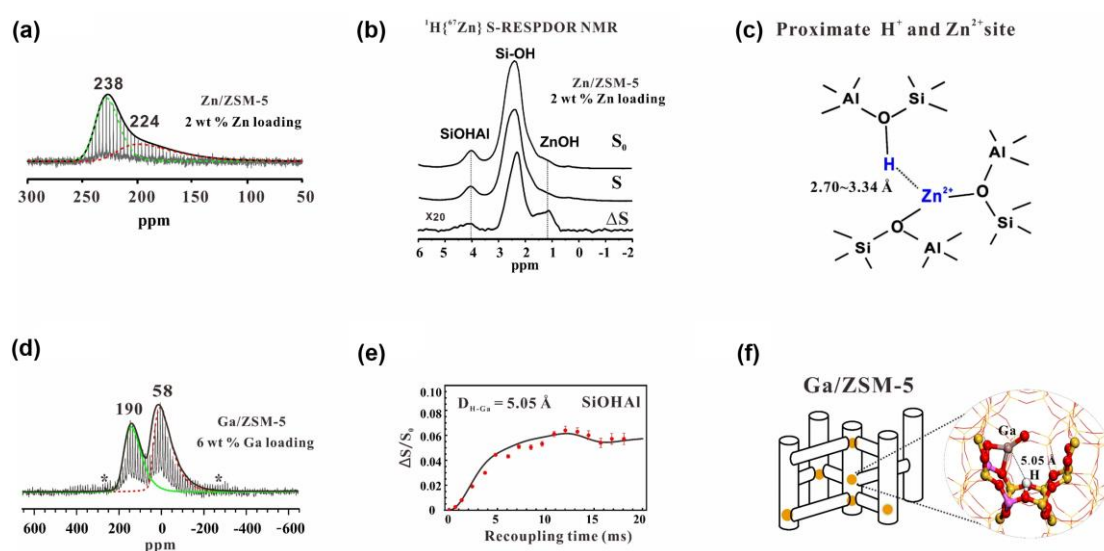

Figure 2. (a) ^{67}Zn HS-QCPMG NMR spectrum of Zn/ZSM-5, (b) ^{1}H-^{67}Zn S-RESPDOR NMR spectrum, and (c) illustration of spatial interaction between Zn species and Brønsted acid site. Reproduced with permission.[21b] Copyright 2016, Wiley-VCH. (d) ^{71}Ga WURST-QCPMG NMR spectrum of Ga/ZSM-5, (e) ^{1}H-^{71}Ga S-RESPDOR build-up curve of Brønsted acidic proton and (f) model of proximate Ga species and Brønsted acid site in ZSM-5 channel. Reproduced with permission.[42] Copyright 2018, American Chemical Society.

The wideband uniform-rate smooth truncation and QCPMG (WURST-QCPMG) [71]Ga NMR and ^{1}H{[71]Ga} S-RESPDOR NMR have been employed to investigate the chemical environments of extra-framework gallium species in Ga-modified ZSM-5 zeolites.[42] Two [71]Ga signals with isotropic chemical shifts at 58 and 190 ppm were resolved in the [71]Ga WURST-QCPMG NMR spectra of Ga/ZSM-5 zeolite (Figure 2d), which can be ascribed to highly dispersed Ga_2O_3 clusters and extra-framework Ga species in the form of GaO^+, respectively. The ^{1}H{[71]Ga} S-RESPDOR NMR and the resulting build-up curve (Figure 2e) suggested the cationic Ga species was involved in the formation of proximate Brønsted acid site-Ga pairs with an internuclear distance being 5.05 Å, consistent with the average [1]H-^{1}H distance between neighboring Brønsted acid sites in H-ZSM-5 (ca. 4.50 Å). This provided detailed information on the location of the Brønsted acid site-Ga pair: sitting on the next-next-nearest-neighboring Al in the 6-membered ring of zeolite channel (Figure 2f).

Based on the S-RESPDOR experiment, a viable NMR method capable of quantitative determination of the synergic active sites was developed, which provides a tool for the analysis of intrinsic activity of the metal-modified zeolites. From the maximum dephasing fraction, residual acidic protons on zeolite, isotopic abundance of metal nuclei and the scaling factor of the ^{1}H dephasing fraction in the [1]H{M} (M: metal) S-RESPDOR experiment, it is possible to determine the concentration of the synergic active sites. This quantification approach is useful for establishing the correlation of the synergic active sites with their catalytic activity in methane activation and methanol-to-aromatics conversion on zeolites.[2f]

Dislodging Al from zeolite framework results in extra-framework Al species, which significantly impacts the catalytic reactions. The formation and nature of extra-framework Al in zeolites was investigated by using multidimensional ^{27}Al MAS NMR spectroscopy.[12a, 43] 2D sensitivity-enhanced ^{27}Al DQ-SQ MAS NMR revealed the detailed evolution of extra-framework Al species and the spatial proximities of various aluminum species in dealuminated HY zeolites.[12a] The strucutres of other extra-framework metal species such as

silver and titanium in zeolites and related materials were examined by SSNMR as well. Popovych and coworkers monitored the changes of silver in AgSi-BEA zeolite as a function of Ag content and thermal treatment by [109]Ag MAS NMR.[44] The full characterization of Ti species in zeolites is essential to understand the detailed property of the Ti active center in heterogeneous catalysis and photocatlysis. [47]Ti/[49]Ti SSNMR has been applied to uncover the titanium environment of fresh and reused titanium-immobilized mesoporous silica nanoparticles.[45] Additionally, [47,49]Ti solid-state NMR has been employed to probe the location and chemical environment of titanium in Ti substituted USY and MFI-type TS-1 zeolites although the spectra feature low resolution because of the low gamma nature and low natural abundance of NMR active [47,49]Ti nucleus.[46] It was found that Ti in the TS-1 framework was essentially tetrahedrally coordinated and became octahedrally coordinated in the presence of water.

3.3 Host-guest interactions and active intermediates in catalytic reactions

The host-guest interaction between organic structure-directing agents and zeolites framework plays essential role in the crystallization and self-assembly during zeolite synthesis. 2D hetero-nuclear correlation SSNMR experiments were used to obtain detailed information on the ordering and arrangement of surfactants confined in FER-type zeolite,[47] ECNU-7P,[48] pure silica MFI zeolite,[49] HOU-4,[50] and mesostructured zeolites.[51] [1]H-^{13}C and [1]H-[29]Si HETCOR experiments confirmed the existence of strong intermolecular interactions between the quaternary ammonium head groups of cetyltriethylammnonium bromide (CTAB) and the ECNU-7P zeolite framework during the self-assembly and structure evolution process.[48] [1]H DQ MAS and ^{1}H triple-quantum (TQ) MAS NMR spectroscopy provided clear evidence for the interaction and connectivity between the internal defect SiOH and organic structure-directing agent in ZSM-12, ZSM-5, and SSZ-74, suggesting that the six-rings are preferred in

the positions near the organic structure-directing agent for the formation of connectivity defects.[52]

The interaction between the guest molecules and the zeolite framework is also a subject of intensive studies regarding molecule diffusion, reactants adsorption, catalytic reactions, and products desorption. SSNMR is powerful tool to characterize the host-guest interactions in zeolites by selectively correlating the interacting nuclei. ^{13}C-^{27}Al double-resonance NMR technique enables direct observation of interactions between the adsorbed or confined organic molecules guest (containing ^{13}C atoms) and zeolite framework host (containing ^{27}Al atoms), by detecting their spatial dipolar ^{13}C -^{27}Al coupling.

The detailed host–guest interaction including the proximity and strength between dealuminated HY and acetone was investigated by ^{13}C–^{27}Al double-resonance NMR.[17b] As shown in the $^{13}C\{^{27}Al\}$ S-RESPDOR NMR spectra of 2–^{13}C-acetone adsorbed on dealuminated HY (**Figure 3a**), the ^{13}C NMR signals in range of 228-234 ppm exhibited a strong ^{13}C–^{27}Al dipolar dephasing. The distances between the carbonyl carbon of acetone and the neighboring framework aluminum were determined to be 3.4 Å by $^{13}C\{^{27}Al\}$ S-RESPDOR NMR build-up curve (Figure 3b). The ^{13}C signals at 228 and 234 ppm due to acetone adsorbed on Brønsted acid site also showed interaction with extra-framework aluminum (as Lewis acid site), as seen in the 2D $^{27}Al\{^{13}C\}$ D-HMQC spectrum (Figure 3c and 3d).

The host-guest interactions introduced by organic molecules in zeolite leads to the formation of supramolecular system.[53] The application of $^{13}C\{^{27}Al\}$ S-RESPDOR experiment coupled with ^{13}C NMR allowed for the characterization of the supramolecular reaction center (SRC) and its reactivity in the methanol-to-olefins (MTO) reaction,[54] which was supposed to be formed by the interaction between Brønsted acid site and trapped hydrocarbon pool (HP) species such as cyclic carbocations and multimethylbenzenes in zeolite. The $^{13}C\{^{27}Al\}$ S-RESPDOR spectra of ^{13}C-methanol reacted over H-ZSM-5 showed that the HP species (0~60

ppm) exhibited different degrees of ^{13}C–^{27}Al dipolar dephasing (Figure 3e), suggesting the spatial interaction between the trapped HP species and Brønsted acid site and the formation of SRC. Further analysis of the ^{13}C–^{27}Al dipole interaction indicated methylbenzenes (MBs) interacted with Brønsted acid site by forming a π-complex, while cyclic carbocations interacted with Brønsted base site by forming an ion-pair complex (Figure 3f). The internuclear spatial interaction between the ^{13}C nuclei from the HP species and the ^{27}Al nuclei from Brønsted acid site dictated the reactivity of the HP species. The function of SRC in the MTO reaction was identified: closer HP species to zeolite framework Al resulted in higher reactivity of the HP species in MTO reaction.[54] Additionally, different interactions associated with the SRC in the MTO reaction were found in ZSM-5, H-SSZ-13, and H-MOR zeolites, revealing the influence of the shape selectivity of zeolites on the host-guest interactions.[55]
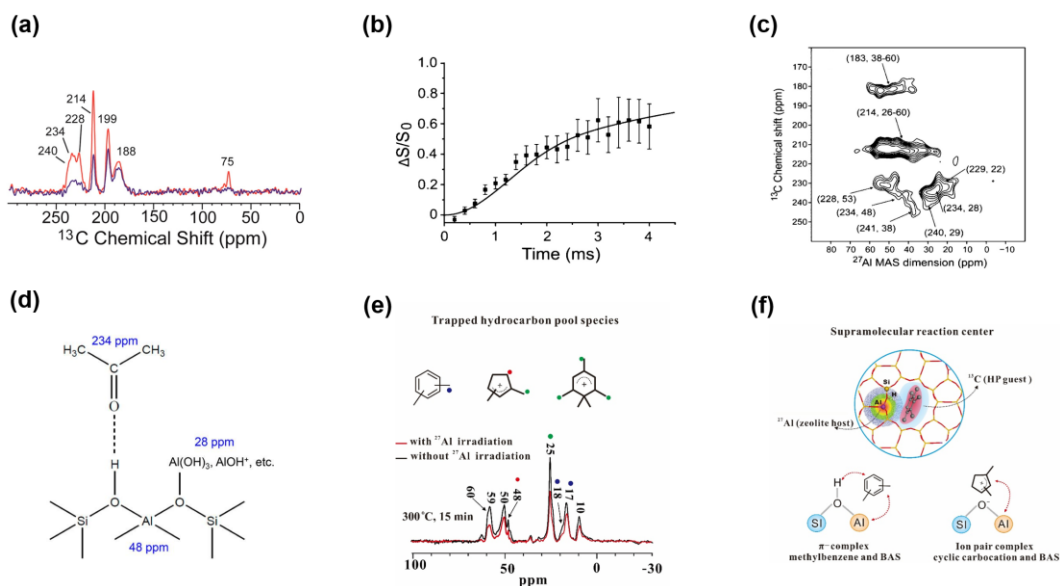

Figure 3. (a) ^{13}C{^{27}Al} S-RESPDOR spectrum of acetone adsorbed dealuminated HY, (b) ^{13}C{^{27}Al} build-up curve of ^{13}C signal at 234 ppm, (c) ^{27}Al{^{13}C} *D*-HMQC spectrum of [2-^{13}C]-acetone loaded on dealuminated HY and (d) schematic model of acetone adsorbed on the Brønsted acid site on dealuminated HY. Reproduced with permission.[17b] Copyright 2014,

American Chemical Society. (e) ^{13}C{^{27}Al} S-RESPDOR spectra of methanol reacted over H-ZSM-5 at 300 and 350 °C for 15 min. (f) Schematic model of supramolecular reaction center. Reproduced with permission.[54] Copyright 2016, Wiley-VCH.

The host-guest interactions on zeolite involving extra-framework Al species has been explored as well.[56] For the MTO reaction on dealuminated H-ZSM-5, a new surface methoxy species bound with extra-framework Al was experimentally identified using ^{13}C{^{27}Al} S-RESPDOR NMR. This species was demonstrated to initiate the direct formation of the first C−C bond product ethene in the MTO reaction. Recently, ^{13}C–^{27}Al and ^{13}C–^{29}Si SSNMR experiments were utilized to probe the interactions between the confined carbenium ions and the zeolite framework during methanol conversion on H-ZSM-5.[57] Considering the importance of the aforementioned metal species on zeolite, it can be envisioned that the characterizations of host-guest interactions by correlating metal nuclei (e.g., Zn, Ga and Sn) and ^{13}C in zeolites would provide deep insights into their properties and catalytic role in reactions.

The observation and identification of active intermediates in zeolite catalyzed reactions is critical for elucidating catalytic reaction mechanism. It is desirable to monitor the species evolution from reactants, to intermediates, and to the final products. To this end, SSNMR particularly in situ NMR show its advantage in the exploration of active species during catalytic process.[58] Numerous reaction intermediates have been successfully discerned by in situ MAS NMR.[58c, 59] Due to the limited NMR detection sensitivity and time scale, the catalytic reactions are often quickly quenched and the frozen intermediates trapped on catalysts are characterized at batch mode. Nevertheless, NMR detection of active intermediates in catalytic reactions at operando condition has attracted increasing attention. [58a, 60]

Figure 4a shows the in situ continuous-flow ^{13}C MAS NMR spectra of ^{13}CH$_3$OH reacted at H-SSZ-13 and SAPO-34, in which two carbenium ions pentaMCP$^+$ and heptaMB$^+$ as important reaction intermediates were clearly identified (Figure 4b).[59c] Very recently, Zhou and co-workers reported the mechanistic study of ethanol dehydration to ethene over H-ZSM-5 by using in situ continuous-flow ^{13}C MAS NMR spectroscopy.[60b] Stable triethyloxonium ion was
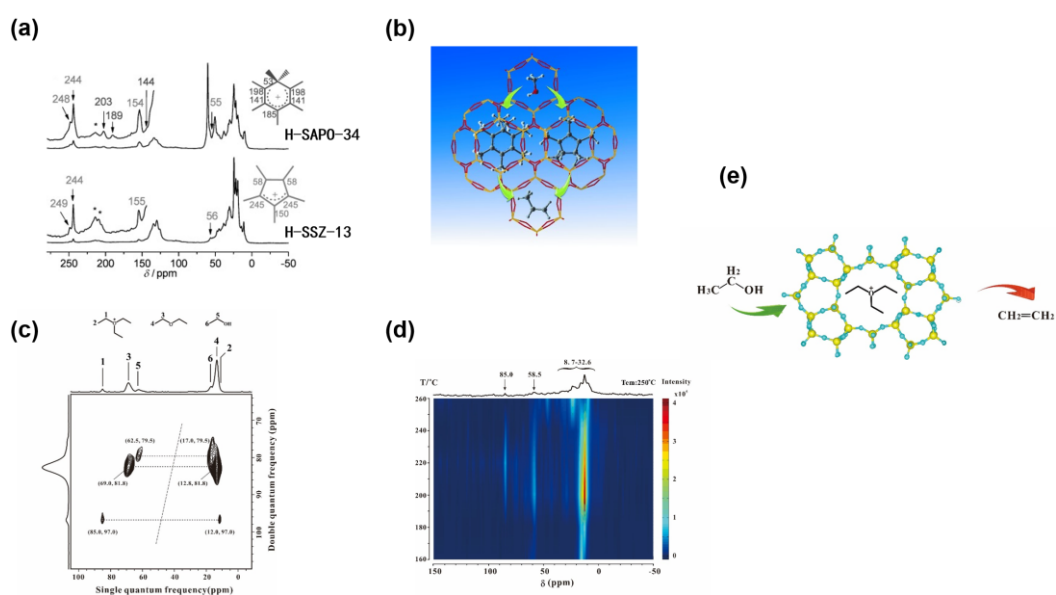

Figure 4. (a) ^{13}C MAS NMR spectra of ^{13}CH$_3$OH reacted at SAPO-34 and H-SSZ-13, and (b) illustration of the formation of heptaMB$^+$ and pentaMCP$^+$ in H-SSZ-13. Reproduced with permission.[59c] Copyright 2013, Wiley-VCH. (c) 2D ^{13}C–^{13}C INADEQUATE MAS NMR spectrum of reaction of ^{13}CH$_3$^{13}CH$_2$OH on H-ZSM-5, (d) real-time in situ ^{13}C MAS NMR of ^{13}CH$_3$^{13}CH$_2$OH dehydration on zeolite H-ZSM-5 as a function of reaction temperatures and (e) illustration of triethyloxonium ion as reaction intermediate in the ethanol dehydration to ethene reaction. Reproduced with permission.[60b] Copyright 2019, Nature Publishing Group.

for the first time observed during the reaction, which was confirmed by 2D ^{13}C–^{13}C INADEQUATE MAS NMR experiment (Figure 4c). The reactivity of this species was

revealed by the in situ ^{13}C NMR experiment at elevated temperatures (Figure 4d). The facile transformation of triethyloxonium ion to ethene product pointed to its intermediate role in the ethanol dehydration process (Figure 4e).

In situ ^{13}C MAS NMR was also used to reveal the first carbon–carbon bond formation mechanism in the methanol-to-hydrocarbons reaction over H-ZSM-5.[60a] The development of novel in situ NMR probe and rotors allowed achieving the study of catalytic reaction with different phase and at high temperature and high pressure condition.[58c] For example, in the work by Jaegers and co-workers,[60c] cyclohexene carbenium ion was discerned as the intermediate in the phenol alkylation with cyclohexanol over zeolite H-Beta in liquid system.

4. SSNMR characterization of MOFs

MOFs are three-dimensionally connected networks consisting of metal centers or metal clusters linked by organic ligands. The vast variety of MOFs have found enormous applications in many areas, including gas storage, chemical separation, molecular catalysis, sensing, and drug delivery.[61] The wide application of MOFs is mainly ascribed to their intrinsic properties such as large surface area, framework flexibility, diverse pore structure and adjustable functional groups. Structural characterization of MOFs is crucial for understanding their structural-property relationships and the rational design of new types of functional materials.

4.1 Local structure of metal centers

SSNMR spectroscopy offers versatile approaches to characterize MOF lattice. The structures of metal centers can be examined by NMR experiments of quadrupolar nuclei including [91]Zr, [25]Mg, [67]Zn, [27]Al, [69/71]Ga,[47/49]Ti, etc. However, the low γ elements, such as [25]Mg and [67]Zn, are difficult for conventional NMR detection. The availability high magnetic field (>18.8 T) coupled with advanced pulse-sequence benefits NMR analysis of these challenging nuclei.

For example, Xu and coworkers applied [25]Mg 2D MQMAS NMR at a magnetic field of 21.1 T and natural abundance to detect the multiple non-equivalent Mg sites in α-Mg_3-$(HCOO)_6$ (**Figure 5a**).[20a] Different correlation peaks corresponding to four distinct Mg sites were clearly resolved in the [25]Mg MQMAS spectrum of the activated α-Mg_3-$(HCOO)_6$ (Figure 5b). The NMR parameters including Qcc, η and δ_{iso} for the activated and organic molecule (DMF and benzene) loaded in α-Mg_3-$(HCOO)_6$ can be accurately determined from the [25]Mg MQMAS NMR experiment.
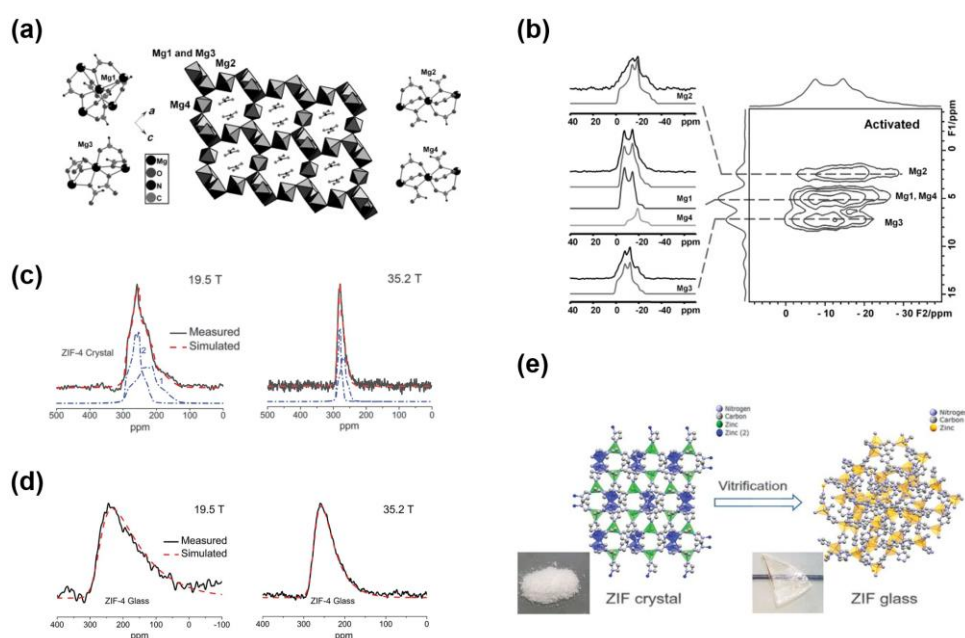

Figure 5. (a) Framework and Mg coordination environments of α-Mg_3-$(HCOO)_6$ and (b) natural abundance [25]Mg 3QMAS NMR spectrum of the activated α-Mg_3-$(HCOO)_6$. Reproduced with permission.[20a] Copyright 2013, Wiley-VCH. [67]Zn MAS NMR spectra of crystalline ZIF-4 (c) and ZIF-4 glass (d) acquired at 19.5 and 35.2 T. (e) Schematic illustration of the structural alternation from crystalline ZIF to its glassy state during melt-quenching. Reproduced with permission.[62] Copyright 2020, American Association for the Advancement of Science.

[67]Zn MAS NMR spectra were highly sensitive to the local Zn environment and employed to differentiate non-equivalent Zn sites in ZIF-8, ZIF-14 and ZIF-4.[20b] Recently, the structural alternation from crystalline ZIFs to their glassy state during melt-quenching treatment has been monitored by ultra-highfield [67]Zn SSNMR spectroscopy.[62] In the [67]Zn MAS NMR spectra of crystalline ZIF-4 and ZIF-4 glass acquired at 19.5 and 35.2 T (Figure 5c), there were two crystallographically distinct Zn sites at a 1:1 ratio in the parent ZIF-4 sample. Upon melt-quenching treatment, the transformation of two distinct Zn sites in the parent ZIF-4 crystal into a single disordered tetrahedral site in the ZIF-4 glass was reflected in the [67]Zn NMR spectra (Figure 5d). A glass formation mechanism was proposed according to the structural change from crystalline ZIFs to their glassy state (Figure 5e).[62]

With respect to the variety of metal elements in framework, other metal nuclei such as [91]Zr,[21a] [47/49]Ti,[21a] [43]Ca,[63] [69/71]Ga,[64], [27]Al[65] have been detected by high-field SSNMR spectroscopy to explore the environment of the metal centers in various MOFs. Furthermore, ^{17}O MAS NMR has been utilized to differentiate the crystallographically nonequivalent oxygen sites in MOFs lattice. In [17]O-enriched UiO-66, three chemically unique oxygens including carboxylate (COO^-) alongside μ_3-O^{2-} anions and μ_3−OH groups were clearly distinguished.[66] Similarly, the carboxylate groups linking with metals and bridging μ_2−OH were well resolved in the ^{17}O MAS NMR spectrum of [17]O-enriched MIL-53.[66-67]

4.2 Local structure of organic linkers

The structures and their functionalities of organic linkers in MOFs can be routinely characterized by ^{1}H, ^{13}C and ^{15}N SSNMR.[10c, 68] The combination of high magnetic field (21.1 T), ultrafast MAS (62.5 kHz) and ^{1}H isotopic dilution protocol enables the unambiguous assignment of complicated ^{1}H and ^{13}C chemical shifts and the structural determination of guest molecules confined in α-Mg-formate.[68a] The influence of chemical linker modification on their ring rotational rates in the functionalized UiO-66 was unraveled by [1]H-^{13}C separated-

local-field (SLF) SSNMR.[69] Specifically, variable-temperatures (VT) ^{2}H NMR provides a versatile approach to measure the rotational frequencies of the linkers and monitor the flexibility and molecular dynamics of various MOFs.[70]

Multivariate MOFs (MTV-MOFs) were fabricated through mixing variable linkers and variable metals ions.[71] In order to establish the structure-property relationships of MTV-MOFs, it is desirable to obtain the spatial arrangements information of various linkers or metal ions. Kong and coworkers determined the spatial apportionment of functional groups in a series of MTV-MOF-5 using SSNMR quantitative distances measurements in combination with molecular simulations.[72] **Figure 6a** shows a representative ^{13}C-^{15}N spin pair between two distinct linkers in ^{15}N isotopically enriched MTV-MOF-5-BF, where the average ^{13}C-^{15}N distances could be extracted from the ^{13}C{^{15}N} REDOR NMR experiments (Figure 6b). By fitting the ^{13}C{^{15}N} REDOR decay curves and calculating the effective interaction energies using Monte Carlo simulations, the spatial apportionment of mixing linkers in MTV-MOF-5-BF was determined to be small cluster (Figure 6c). Theoretical prediction of the CO_2 adsorption isotherms compared with the corresponding experimental data further confirmed the spatial apportionment of mixing linkers in MTV-MOFs. This work provided a viable strategy to resolve apportionment in disordered MTV-MOFs through inter-linker hetero-nuclear distance measurements.
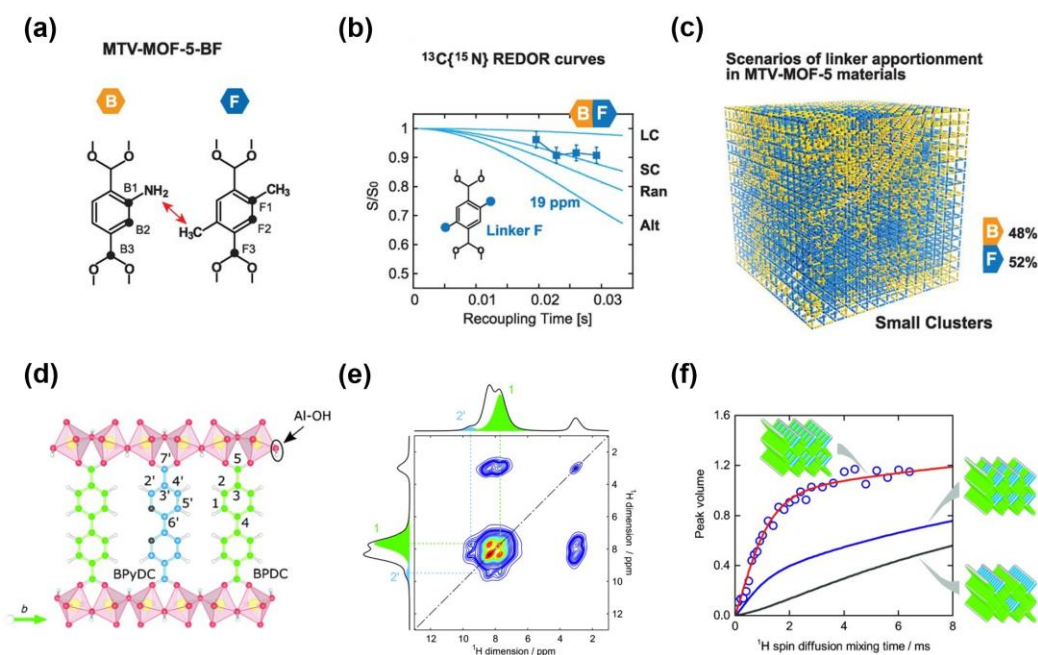
Figure 6. (a) The specified ^{13}C-^{15}N spin pair is indicated in MTV-MOF-5-BF, (b) fitting of experimental $^{13}C\{^{15}N\}$ REDOR decay curves using different models, large clusters (LC), small clusters (SC), random (Ran), and alternating (Alt) and (c) the derived apportionments for the MTV-MOF-5-BF. Reproduced with permission.[72] Copyright 2013, American Association for the Advancement of Science. (d) Labeling of carbon and hydrogen atoms of ML-DUT-5. (e) 2D ^1H spin-diffusion MAS NMR spectrum of ML-DUT-5. (f) Experimental and calculated ^1H spin-diffusion buildup curves of ML-DUT-5. Reproduced with permission.[73] Copyright 2015, Wiley-VCH.

The spatial distribution of the mixed linkers in MTV-MOFs could also be elucidated from ^1H spin-diffusion SSNMR measurements whereas the ^{15}N isotope enrichment of MTV-MOFs is unnecessary.[73] Figure 6d shows the labeling of carbon and hydrogen atoms of ML-DUT-5, which contained biphenyl dicarboxylic acid (BPDC) and bipyridyl dicarboxylic acid (BPyDC) linkers. In the 2D ^1H spin-diffusion MAS NMR spectrum of ML-DUT-5 (Figure 6e), the cross correlation peaks between the H1 site of BPDC and H2' site of BPyDC were clearly observable. The existence of the cross peaks suggested that BPyDC and BPDC linkers

partially shared the same crystallites. Three models with different linkers apportionments were proposed to fit the ^1H-^1H spin diffusion buildup curves (Figure 6f). It is clear that only the model in which BPyDC and BPDC linkers are homogeneously distributed within the framework agreed well with the experimental results.[73] The work shows that high resolution ^1H spin-diffusion MAS NMR experiment is simple but robust to explore the spatial distribution of mixed linkers in MOFs.

Advanced SSNMR methods were developed to improve the ^1H spectral resolution and explore the spatial apportionments of MTV-MOFs. Carbon-detected version of the proton spin-diffusion NMR experiment was recently used to effectively improve NMR detection resolution and thus yield structural information of mixed-linker UiO-66-type metal-organic material.[74] Moreover, high resolution ^1H CRAMPS spin diffusion SSNMR in combination with computational modeling was employed to elucidate structural arrangements and determine the short-range order (SRO) parameter of mixed-linkers in ZIF-8 and ZIF-90.[75]

4.3 Host-guest interactions between confined gas molecule and MOFs

4.3.1 Hydrogen and light alkanes in MOFs

MOFs exhibit promising capability of adsorption and storage of the clean energy gas including hydrogen and methane. In order to fabricate new types of MOFs to enhance storage capacity, detailed knowledge of the host-guest interactions and the mobility of gas molecules confined inside MOFs is required. SSNMR is particularly suitable for characterization of the interaction between host framework and adsorbed molecules as well as the dynamics of the latter. ^2H SSNMR is in particular a powerful probe for this purpose.

Huang and coworkers investigated the hydrogen adsorption in UiO-66 and M-MOF-74 (M = Zn, Mg, Ni) using VT ^2H SSNMR.[76] The static VT ^2H NMR spectrum of D_2 in Mg-MOF-74 as shown in **Figure 7a** exhibited a narrow peak in range of 253~293 K, suggesting highly mobile D_2 exhibiting rapid isotropic reorientation in Mg-MOF-74 at the temperature range. The ^2H NMR signal became broad as the temperature decreased to 173 K, indicative of onset

of D_2 adsorption on Mg-MOF-74. At 153 K, the adsorbed D_2 (broad power pattern) and free D_2 (narrow central peak) coexisted inside the Mg-MOF-74 pore (Figure 7a). The fitting of the wide ^2H lineshapes at 133 K revealed that D_2 exhibits a local wobbling rotation with respect to the open metal site (OMS) as well as a non-localized six-site hopping along the pore edge (Figure 7b). The VT ^2H NMR spectra of D_2 adsorbed on UiO-66 and Zn-MOF-74 exhibited narrow ^2H resonances, indicating rapid reorientation of the D_2 molecules and weaker interaction between D_2 and frameworks.[76] Therefore, the VT ^2H NMR of D_2 adsorption on MOFs provided detailed information on H_2 dynamics and its host-guest interactions with MOFs.
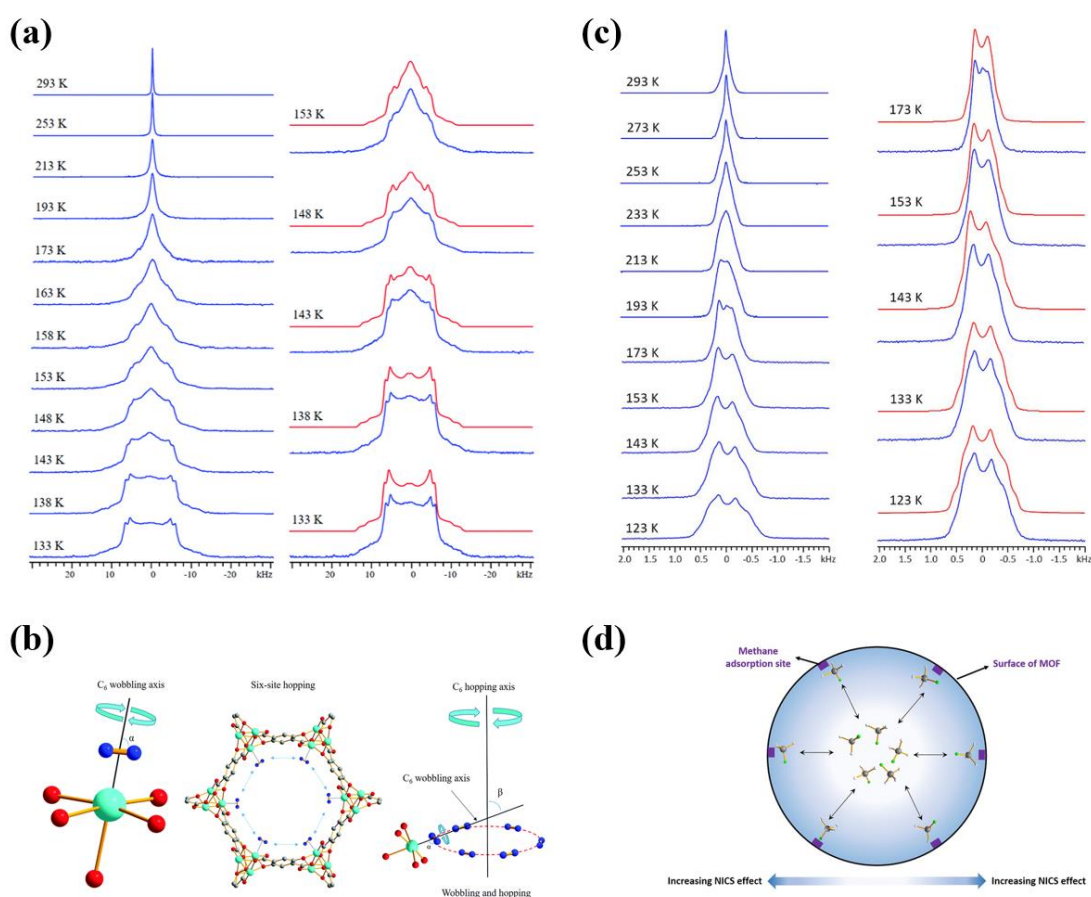

Figure 7. (a) Experimental (blue) and simulated (red) VT ^2H NMR spectra of D_2 adsorbed in Mg-MOF-74, (b) localized wobbling and six-site hopping of D_2 molecules adsorbed on the open metal site of MOF-74. Reproduced with permission.[76] Copyright 2016, Royal Society

of Chemistry. (c) Experimental (blue) and simulated (red) VT ^{2}H NMR spectra of CH_3D adsorbed in α-$Mg_3(HCO_2)_6$ and (d) simplified illustration of the Nucleus-Independent Chemical Shift (NICS) effect on methane adsorbed in MOFs. Reproduced with permission.[77] Copyright 2018, Wiley-VCH.

^{2}H NMR offers a straightforward method for the investigation of methane adsorption locations and dynamics within MOFs pores.[78] Methane adsorption behavior on several representative MOFs has been examined by VT ^{2}H NMR spectroscopy.[77] Figure 7c displayed the static VT ^{2}H static NMR spectra of singly deuterated methane (CH_3D) adsorbed on α-$Mg_3(HCO_2)_6$. At 293 K, a sharp resonance corresponds to rapidly and isotropically tumbling CH_3D. ^{2}H powder patterns was clearly observable at 123~173 K, ascribed to adsorbed CH_3D. The relatively narrow ^{2}H NMR linewidth at 123 K was resulted from the fast exchange between CH_3D experiencing isotropically tumbling and adsorbed CH_3D undergoing anisotropic motion. As CH_3D molecules approach and adsorb on the MOF surface, the increase of Nucleus-Independent Chemical Shift (NICS) magnitude indeced pronounced ^{2}H CSA of CH_3D (Figure 7d). According to the determined C_Q values of CH_3D adsorbed on MOFs at low temperature, Mg-MOF-74 shows the weakest methane binding strength compared to that of α-$Mg_3(HCO_2)_6$, α-$Zn_3(HCO_2)_6$, and SIFSIX-3-Zn.[77]

SSNMR enables direct investigation of adsorbed light alkanes in MOFs. The host-guest interaction and primary adsorption site of light alkanes (methane, ethane, and propane) confined inside UiO-67 and MTV-UiO-66 was revealed by ^{1}H-^{1}H spin diffusion SSNMR experiments.[79] Methane diffusion in $M_2(dobdc)$ as different methane loadings was investigated by PFG Stimulated Echo NMR and MD simulations. It was found that the self-diffusion coefficient of methane in $M_2(dobdc)$ was inversely related to the binding energy at the unsaturated metal sites.[80]

4.3.2 CO$_2$ in MOFs

MOFs exhibit great potential for CO_2 capture to cut down greenhouse gas emissions owing to their large gas adsorption capacities and ability to selectively separate CO_2 from gases mixtures. Understanding of dynamic behavior of adsorbed CO_2 is important for the practical application of MOFs as adsorbents. The dynamics of CO_2 in the Mg-MOF-74 was revealed by the analysis of ^{13}C static NMR line shapes and spin−lattice relaxation times.[6] It was found that CO_2 preserved uniaxial rotation with a fixed rotation angle along the rotation axis of Mg−O(CO_2) vector in Mg-MOF-74. The motion of CO_2 and the interactions with framework in various MOFs were comprehensively studied by VT ^{13}C static NMR experiments.[81]

Diamine-appended MOFs are highly efficient for CO_2 adsorption from various gas mixtures.[82] Recently, multinuclear SSNMR spectroscopy has been utilized to characterize CO_2 chemisorption in diamine-appended metal-organic frameworks.[83] **Figure 8a-8b** shows the ^{13}C and ^{15}N CP/MAS NMR spectra of dmpn−Mg$_2$(dobpdc) upon adsorption of CO_2, confirming the formation of ammonium carbamate and carbamic acid in Mg$_2$(dobpdc) channel. The detailed assignments in the ^1H-^{13}C HETCOR spectrum (Figure 8c) of CO_2 adsorbed on dmpn−Mg$_2$(dobpdc) was manifested in Figure 8d. The ^1H-^{13}C HETCOR spectrum shows identification of the adsorption sites by correlating the C atoms from CO_2 with the H atoms from different NH groups on framework. (Figure 8c) The detailed NMR assignments with the assistance of DFT theoretical calculations in the ^1H-^{13}C HETCOR spectrum of CO_2 adsorbed on dmpn−Mg$_2$(dobpdc) were manifested in Figure 8d. It should be noted that the hydrogen of the carbamic acid −OH group is in spatial proximity to the carbon site of the ammonium carbamate. On the basis of the NMR observations and computational CO_2 adsorption energies, a mixed chemisorption structure was proposed (Figure 8e). The formation of a 1:1 mixture of ammonium carbamate and carbamic acid resulted in highly efficient CO_2 adsorption properties of dmpn−Mg$_2$(dobpdc).[83]
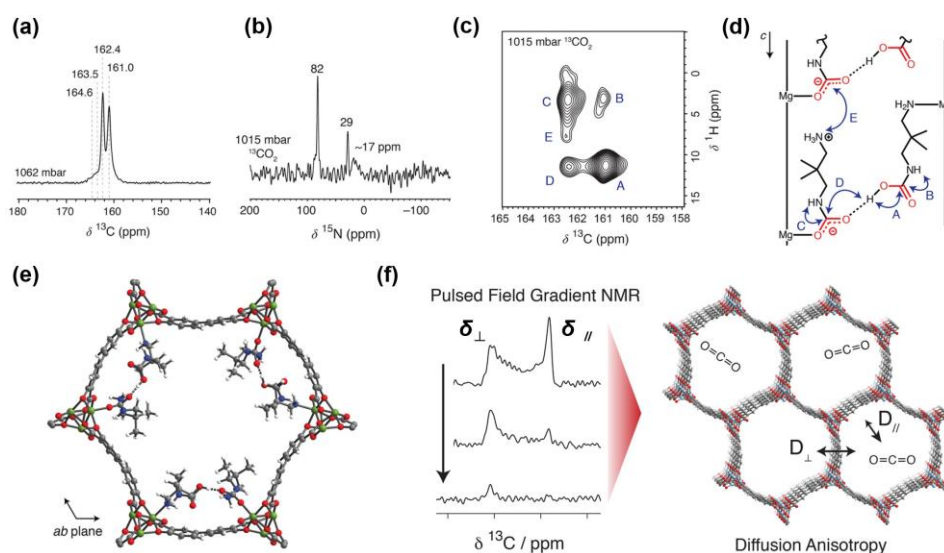
Figure 8. (a) $^1H \rightarrow {}^{13}C$ and (b) $^1H \rightarrow {}^{15}N$ CP/MAS, and (c) ^1H-^{13}C HETCOR NMR spectra of dmpn−Mg$_2$(dobpdc) upon CO$_2$ adsorption. (d) Detailed assignments for the ^1H-^{13}C HETCOR correlations. (e) Proposed mixed chemisorption structures with ammonium carbamate and carbamic acid in a 1:1 ratio. Reproduced with permission.[83] Copyright 2018, American Chemical Society. (f) Two CO$_2$ diffusion pathways in Zn$_2$(dobpdc) as determined by ^{13}C PFG NMR. Reproduced with permission.[84] Copyright 2018, American Chemical Society.

SSNMR provided a deeper understanding of CO$_2$ adsorption within diamine−M$_2$(dobpdc) compounds, which benefits the design of improved materials for the CO$_2$ capture. The detailed interactions between CO$_2$ and dmpn−Mg$_2$(dobpdc), 2-ampd−Mg$_2$(dobpdc) were investigated by means of ^1H and ^{13}C MAS NMR spectroscopy as well.[85] It is interesting to note that water molecules enhance CO$_2$ capture in oxidation-resistant 2-ampd−Mg$_2$(dobpdc) through hydrogen-bonding interactions with the ammonium carbamate chains formed upon CO$_2$ adsorption.[85a] Additionally, the host-guest interactions between alcoholamine- and alkoxyalkylamine-functionalized Mg$_2$(dobpdc) and CO$_2$ were explored using ^{13}C and ^{15}N CP/MAS as well as ^1H-^{13}C HETCOR NMR to clarify the cooperative chain-forming mechanisms towards energy-efficient CO$_2$ separations.[86]

Insight into the long-range diffusive motion of confined molecules within the nanosized pores of MOFs is critical for guiding the design of robust materials with improved gas transport properties. Pulsed field gradient (PFG) NMR spectroscopy that is a well-established technique for the measurement of intracrystalline self-diffusion in porous materials was used to study the diffusion of CO_2 within the pores of $Zn_2(dobpdc)$.[84] Self-diffusion coefficients were determined by the analysis of the ^{13}C NMR line shape as a function of the applied field gradient. ^{13}C PFG NMR in combination with molecular dynamics (MD) simulations revealed unexpected CO_2 diffusion: in addition to the diffusion through the channels parallel to the crystallographic c axis, CO_2 diffused between the hexagonal channels due to the presence of framework defects in the crystallographic ab plane (Figure 8f). The work demonstrated an example for the measurement of the self-diffusion in different crystallographic directions in MOFs from residual chemical shift anisotropy for pore-confined CO_2 using PFG NMR spectroscopy. The results also show the importance of defects for multidimensional CO_2 transport particularly in MOFs one-dimensional porosity.

5. SSNMR investigation of COFs

COFs constructed by the covalent linkage of building units represent a new class of porous polymers with high chemical and thermal stability and well-defined structures.[87] COFs show great potential for a range of applications in gas storage, chemical separation, chemical sensor, energy conversion and molecular catalysis. The chemical composition of COFs has been comprehensively characterized by multinuclear SSNMR. $^1H{\rightarrow}^{13}C$ CP/MAS NMR serves as a robust and straightforward tool to characterize the functional groups in various COFs.[88] ^{13}C NMR chemical shifts of the synthesized COFs and starting monomers can be directly compared to assess the introduction of functional groups to COFs. ^{13}C CP/MAS NMR spectroscopy verified the anticipated covalent bonding with atomic-level precision and high crystallinity in the structure of large single crystals of 3D imine-based COFs including COF-

300, COF-303, LZU-79, and LZU-111.[88h] In addition to ^{13}C MAS NMR, ^{11}B, ^{15}N MAS

NMR and ^{129}Xe NMR have also been utilized to elucidate the local framework structure and

pore property of various COFs.[89] Three consecutive transformations in porous, crystalline

cyclic carbamate and thiocarbamate-linked frameworks through postsynthetic modifications

of imine-linked COF-170 were identified from $^1H \rightarrow ^{15}N$ CP/MAS NMR spectroscopy.[89b] The

local structure of ionic covalent organic framework (ICOF) capable of transporting lithium

ions was characterized by ^{13}C and ^{11}B MAS NMR. [90] The structural transformation and

dynamic behavior of a new 3D COF LZU-301 was observed using ^{129}Xe NMR spectroscopy,

in which a gradual switch of ^{129}Xe NMR signal from high field to low field indicated a state

transition from contracted LZU-301 to expanded form.[89d]

The detection sensitivity and spectral resolution is often problematic in the SSNMR

characterization of COFs, since the framework elements, such as ^{15}N, have low natural

abundance (0.37 %) and low γ, leading to low NMR detection sensitivity. DNP is a technique

of choice for COFs due to its capability of signal enhancement by 2−3 orders of magnitude.

Cao and coworkers constructed a radical-embedded COFs which allows for DNP

enhancement without introducing extraneous polarizing agents.[91] **Figure 9a** shows the

illustration of chemical structure of PR(x)-COFs containing proxyl radical (PR) and reduced

form of PR, in which the radical concentration can be explicitly adjusted. A high resolution

DNP-enhanced $^1H \rightarrow ^{13}C$ CP/MAS spectrum of PR(10)-COF was obtained with a DNP
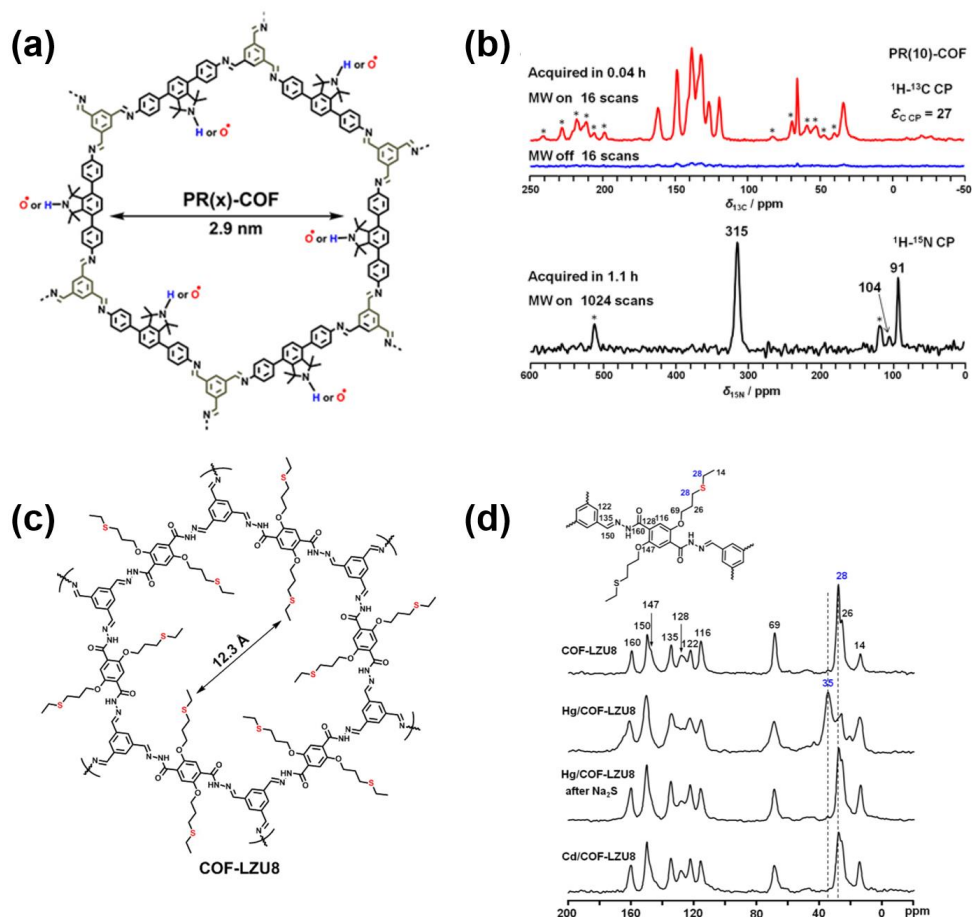
enhancement factor of

Figure 9. (a) Schematic structure of PR(x)-COFs, (b) DNP-enhanced $^1H\rightarrow{}^{13}C$ and $^1H\rightarrow{}^{15}N$ CP/MAS NMR spectra of PR(10)-COF (^{13}C spectrum without DNP is displayed in blue), Reproduced with permission.[91] Copyright 2018, American Chemical Society. (c) Schematic structure of COF-LZU8 and (d) ^{13}C CP/MAS NMR spectra of COF-LZU8, Hg/COF-LZU8, Hg/COF-LZU8 after the treatment with Na$_2$S, and Cd/COF-LZU8. Reproduced with permission.[92] Copyright 2016, American Chemical Society.

~27 (Figure 9b). The resonances at 91, 104, and 315 ppm assigned to −N−H, terminal −NH$_2$, and –N=C− sites, respectively, can be clearly distinguished in the DNP-enhanced $^1H\rightarrow{}^{15}N$ CP/MAS NMR spectra, whereas these signals cannot be observed without DNP. The extraneous polarizing agent such as a stable organic radical is typically required in the DNP experiments. This work provided a strategy for direct construction of radical COFs from radical monomers suitable for direct DNP NMR characterization, which circumvents the

problem caused by the chemical compatibility between the polarizing agent and the sample that has to be addressed in the conventional DNP approach.

SSNMR exhibits potential for exploring the host-guest interaction mechanism in COFs. Ding and coworkers[92] fabricated a thioetherfunctionalized COF material, COF-LZU8, for selective detection and facile removal of highly toxic mercury(II). COF-LZU8 showed strong fluorescence upon excitation at 390 nm, which was quenched after introducing Hg^{2+} to the material. The $^1H \rightarrow {}^{13}C$ CP/MAS NMR spectrum of COF-LZU8 showed that the peak at 28 ppm assigned to the methylene carbons adjacent to the S atoms in COF-LZU8 was obviously shifted to 35 ppm upon the adsorption of Hg^{2+} (Figure 9d), while the chemical shifts of the other signals remained unchanged. This provided evidence for the strong interaction between S and Hg^{2+} in Hg/COF-LZU8. The treatment of Hg/COF-LZU8 with Na_2S removed Hg^{2+} allowing the recycling of COF-LZU8. This Hg^{2+} elimination was reflected by the recovery of the ^{13}C CP/MAS NMR spectrum (Figure 9d). The introduction of other ions, such as Cd^{2+}, into COF-LZU8 was examined using ^{13}C CP/MAS NMR spectrum as well (Figure 9d). As indicated in this work, ^{13}C CP/MAS NMR was deomstrated to be an effective tool for probing the interaction between metal ions and the functional groups in COFs, which is critical for understanding the adsorption and separation property of porous material as adsorbents.

More information about the interaction between COFs and guest molecules can be obtained from multinuclear and multidimensional SSNMR. Solid-state transverse relaxation T_2 measurement and 2D ^1H-^1H DQ MAS NMR spectroscopy revealed the location and dynamic of inserted PEO chains in COFs. These chains were responsible for the fast ion conductivities and transportation as well as the COF structural stability.[93] The detailed interactions between small organic molecules and the COFs framework were investigated using multidimensional and multinuclear SSNMR as well. 2D ^1H-^1H DQ MAS NMR experiments showed the presence of strong host−guest interaction between residual mesitylene solvent and the framework in both the AB staggered and AA eclipsed polymorphs of COF-1, which plays an

important role in the phase change.[94] The stabilization effects mechanism of pyridine on the structure of COF-5 and COF-10 were revealed by $^1H\rightarrow{}^{15}N$ CP/MAS NMR and 2D ^{11}B MQMAS NMR spectroscopy, in which pyridine formed a Brønsted-type interaction with both COF-5 and COF-10.[95]

MOFs and their derivatives, and COFs are emerging as important catalysts in thermocatalysis, electrocatalysis, photocatalysis due to their adjustable acid property. [96] SSNMR has exhibited great potential for exploring the acidic features of active sites and elucidating the catalyzed reaction mechanism. [97] The detailed structure and the superacidity characteristic of Brønsted acid site in sulfated MOF-808 as solid acid catalyst for dimerization of isobutene were comprehensively examined by SSNMR in conjunction with probe molecule techniques. [97a, b] Using SSNMR and deprotonation energy calculations, the phosphorus chemical environment and the acidic property of phosphonate-modified UiO-66 as Brønsted acid catalyst for biomass conversion were determined. [97c] TADDOL-embedded chiral porous polymer (TADDOL-CPP) can act as a highly efficient and recyclable catalyst in the asymmetric addition of diethylzinc to aromatic aldehydes. The key intermediates formed upon the reaction of ^{13}C-labeled benzaldehyde reactant were identified and thus the detailed catalyzed reaction mechanism was revealed accordingly.[97d]

6. SSNMR characterization of other microporous materials

6.1 PAFs

PAFs built by C-C aromatic-based building units hold great promise for gas storage and capture because of their ultra-high surface area and high physicochemical stability.[98] Multinuclear ^1H, ^{13}C, and ^{29}Si SSNMR has been efficiently employed for structural characterization of various PAFs including PAF-1,[99] PAF-5,[100] JUC-Z2,[101] JUC-Z12,[102] mPAF-1,[103] sulfonated PAFs[104] and PAFPORP[105]. PFA-1 possesses high surface area of 7100 m^2/g and exceptional thermal/hydrothermal stabilities. The local diamond-like

tetrahedral bonding of tetraphenylene methane building unit in PAF-1 was resolved by ^{1}H MAS, ^{1}H$\rightarrow$^{13}C CP/MAS, and 2D ^{1}H-^{13}C HETCOR NMR spectra.[99] ^{1}H$\rightarrow$^{13}C CP/MAS NMR and ^{29}Si MAS NMR experiments was employed to characterize the structure of JUC-Z1 capable of selectively adsorbing benzene[106] as well as PAF-3 and PAF-4 with excellent adsorption ability to hydrogen, methane and carbon dioxide.[107] Recently, Li and coworkers[108] constructed PAF-100 and PAF-101 with high surface areas, large pore volumes, and high performance of methane uptakes. ^{1}H$\rightarrow$^{13}C and ^{1}H$\rightarrow$^{29}Si CP/MAS NMR experiments suggested the uniform distribution of carbon and silicon sites in the framework units. VT ^{2}H spin-echo SSNMR has been utilized to explore the dynamics of p-phenylene rotors of [D$_4$]PAF-3 framework, in which the rotational rates and the librational amplitude at high temperature were determined.[109] The constructive elements (p-phenylene) of the [D$_4$]PAF-3 are robust struts and ultra-fast rotors. The rotational motion of p-phenylene rotors can be actively regulated by controlling the temperature and the presence of guest molecule. It is noteworthy that the adsorption and desorption of I$_2$ can effectively regulate the rotor speed of [D$_4$]PAF-3. ^{2}H NMR spectroscopy revealed that the rotational rate of p-phenylene of [D$_4$]PAF-3 drastically slowed down as I$_2$ diffused into the PAF-3 pores due to the presence of I$_2$–phenylene interactions.[109]

6.2 Porous layered materials

6.2.1 Graphene derivatives

Porous layered materials including inorganic and organic open frameworks have been extensively developed and studied due to their great potential and tremendous applications in catalysts, sorbents and electronic devices, etc. The porous layered materials, such as montmorillonite[110] and sodium disilicate[111], have been studied with SSNMR. The recent progress regarding the SSNMR characterization of 2D layered graphene derivatives, layered double hydroxides (LDHs) and layered silicates is briefly described in the following sections.

Graphene derivatives, such as graphene oxide (GO), is an important class of 2D layered materials with a wide range of application in energy storage and conversion devices, separation membranes due to their outstanding electrical, optical, thermal, and mechanical properties.[112] The interlayer spacing of graphene derivatives can be well controlled by introducing diamine pillars to adjust their molecular selectivity, permeability and ionic conductivity. SSNMR has been utilized to probe the cross-linking interaction between pillared graphene and diamine.[113] **Figures 10a** shows the $^1H \rightarrow ^{13}C$ CP/MAS NMR spectra of GO and unreduced pillared materials (6-Ps). After introduction of 1,6-diaminohexane, the ^{13}C NMR signals from the C−O−C epoxides and C−OH hydroxyls in 6-Ps significantly decreased relative to GO due to covalent attachment of pillar molecules with GO sheets. The appearance of the ^{15}N signal in range of 100~200 ppm due to reacted amides verified that the pillar molecule was covalently grafted (Figure 10b). Further ^{13}C-^{15}N HETCOR spectrum (Figure 10c) provided additional experimental evidence for the cross-linking interaction. The appearance of the correlation peaks between amide nitrogen ($\delta_{15N} \sim 110-170$ ppm) and amide
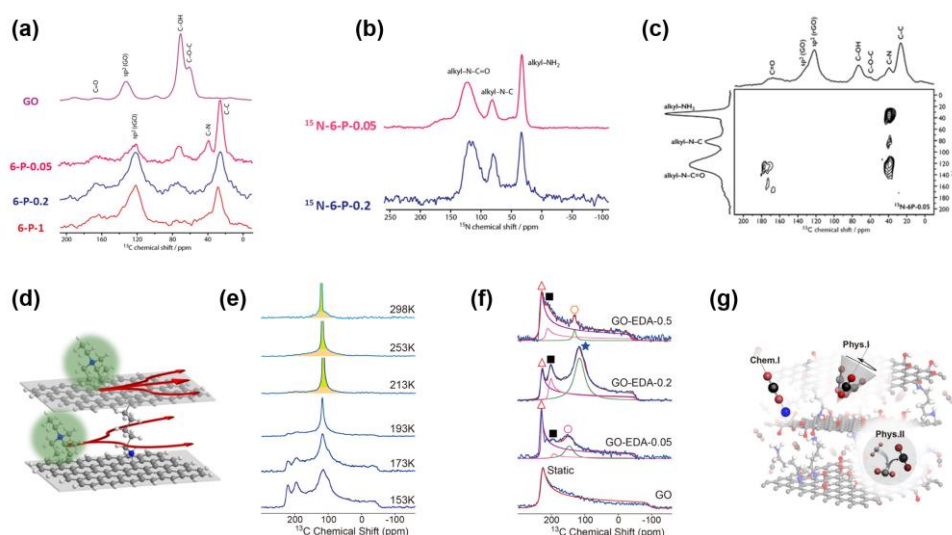

Figure 10. (a) $^1H \rightarrow ^{13}C$ CP/MAS NMR spectra of graphene oxide (GO) and unreduced pillared materials (6-Ps) with varied diamine amount, (b) $^1H \rightarrow ^{15}N$ CP/MAS NMR spectra of ^{15}N-labeled 6-P-0.05 and 6-P-0.2, (c) ^{13}C-^{15}N HETCOR NMR spectrum of 6-P-0.05 and (d)

schematic representation of cross-linking interaction. Reproduced with permission.[113] Copyright 2019, American Chemical Society. Static ^{13}C NMR of $^{13}CO_2$ in (e) GO−EDA-0.2 under elevating temperatures and (f) GOs with different EDA loadings at 153 K. (g) graphic illustration of CO_2 adsorbed in diamine-cross-linked GO layers. Reproduced with permission.[114] Copyright 2019, American Chemical Society.

C=O ($\delta_{13C} \sim 165-180$ ppm) suggested that the diamines have reacted with the carboxyl functions on the GO sheets. The C−N pillar carbons ($\delta_{13C} \sim 40$ ppm) are correlated with the N site in α-position to carbons ($\delta_{15N} \sim 83$ ppm), indicating that diamine was grafted to the graphene surface through reactions with epoxides. The pillared graphene materials constructed by cross-linking the graphene sheets with a bifunctional pillar molecule (Figure 10d) facilitated ion transportation and storage capacity for supercapacitors. A sparse filling of pillars in the galleries improved the supercapacitors performances with higher capacitances and larger power capability.

The interlayer spacing of GO with diamine can be utilized for the capture of greenhouse gas CO_2. The introduction of cross-linking molecules leads to complicated host-guest interactions between CO_2 and GO matrix. Cai and coworkers conducted in situ ^{13}C NMR to investigate the adsorption mechanism of CO_2 on diamine-cross-linked GO with controllable interlayer spacing.[114] The ^{13}C NMR CSA pattern served as an effective probe of molecular dynamics of confined CO_2. In the VT static ^{13}C NMR spectra of $^{13}CO_2$ adsorbed on GO− ethylenediamine (EDA)−0.2 (Figure 10e), the spectra consisted of a broad component arising from adsorbed CO_2 and the sharp component associated with gas phase CO_2 at temperature above 213 K. The CSA pattern of adsorbed CO_2 broadens below 193 K, suggesting the presence of restricted motion at that temperature point. For CO_2 adsorbed on the GOs with different EDA loadings, the ^{13}C CSA patterns of adsorbed CO_2 can be deconvoluted into several components (Figure 10f). As manifested in Figure 10g, both physically and chemically adsorbed CO_2 were present

in diamine-cross-linked GO matrices. Phys. I type CO_2 was trapped by electrostatic interactions and undergone uniaxial rotation which was not significantly affected by the interlayer spacing, whereas Phys. II CO_2 was only restricted by van der Waals interactions and exhibited isotropic motion. Chem. I type corresponded to CO_2 chemically interacting with diamines. The interlayer spacing of GOs played a key role in the CO_2 adsorption, resulting in the elevation of CO_2 uptake.

The host-guest chemistry in graphene oxide derivatives is also of great interest for SSNMR investigations.[115] $^1H \rightarrow {}^{13}C$ CP/MAS NMR and 2D ^1H-^{13}C HETCOR NMR experiments provided direct evidence for the reaction between graphene oxide and amine functions occurring via ring opening of the epoxides and ruled out the possibility of amidation reactions with amine derivatives.[115b] The distribution and variation pattern of electrolyte ions including weakly and strongly adsorbed BF_4^- in graphene-film electrodes were revealed by ^{11}B MAS NMR, which shed insights into the fabrication of high performance graphene-film based electric double layer capacitors.[115d]

6.2.2 LDHs

LDHs is a type of inorganic supramolecular materials, which is widely applied in environmental, energy, catalysis, and biomaterials.[116] Detailed information on the local structure of the metal hydroxide layers is prerequisite for assessing their properties and performances. Different Mg local environments in the LDHs with various Al for Mg substitution levels have been uncovered by Sideris and co-workers[117] using high resolution ^{25}Mg MAS NMR spectroscopy. Three different magnesium environments were revealed in the 2D ^{25}Mg MQMAS NMR spectrum of MgAl-19-NO^{3-} (**Figure 11a**). The three signals resolved at 26.6, 40.6 and 47.5 ppm in the F_1 dimension indicated the presence of $Mg(OMg)_6$, $Mg(OAl)_3(OMg)_3$ and $Mg(OAl)_2(OMg)_4$ units, respectively. The relative ratio for the three distinct components was quantitatively determined from the ^{25}Mg MAS NMR spectra with

the input of the NMR parameters (δ_{iso}, Q_{cc} and η_Q) extracted from the ^{25}Mg MQMAS NMR spectra.[117]

The inter-nuclear proximities and cation-ordering of LDHs can be determined using SSNMR spectroscopy. ^{1}H MAS and ^{1}H{^{27}Al}TRAPDOR NMR experiments were conducted on deuterated MgAl-25.1 (Figure 11b).[118] Deuterated samples were used to obtain high-resolution ^{1}H NMR spectra by reducing the ^{1}H-^{1}H dipole-dipole interaction. Different species including Mg$_3$OH (1.1 ppm), Mg$_2$AlOH (2.9 ppm) and water molecule (4.6 ppm) were resolved on the ^{1}H NMR spectra. Two structural units (Mg$_3$OH and Mg$_2$AlOH) can be identified by the different ^{1}H-^{27}Al dipolar dephasing in the ^{1}H{^{27}Al}TRAPDOR spectra (Figure 11b). The mole percentage of Mg$_2$AlOH increased linearly at the expense of Mg$_3$OH as the increase of aluminum loading, suggesting the absence of Al−O−Al linkage in the LDHs (Figure 11c). The high resolution ^{1}H and ^{1}H{^{27}Al} TRAPDOR NMR experiments revealed the local structure and cation orderings of LDHs.[118]
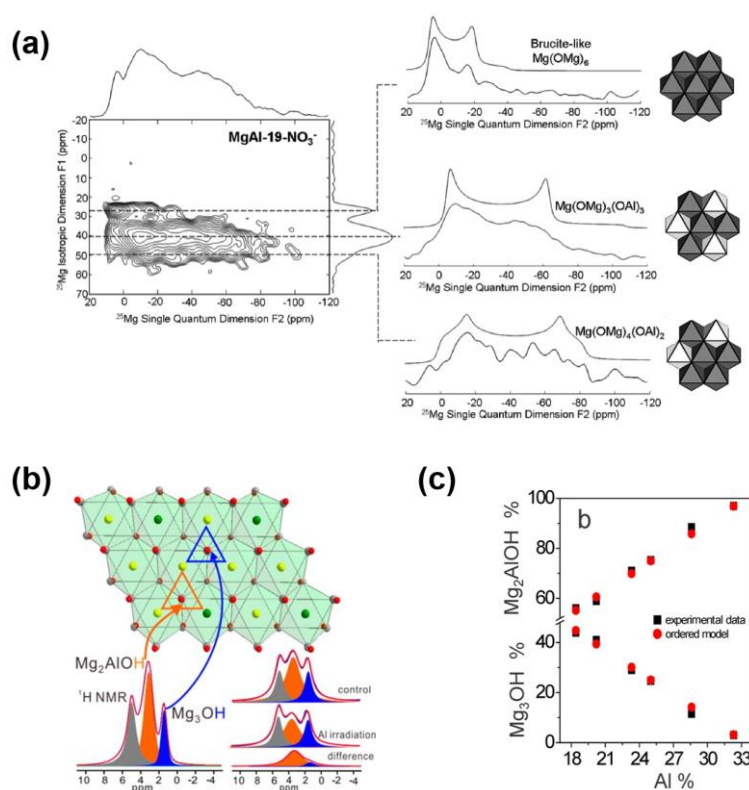
Figure 11. (a) Natural abundance ^{25}Mg MQMAS spectrum of MgAl-19-NO$_3^-$ (19% of Mg^{2+} is substituted by Al^{3+} and NO$_3^-$ is the interlayer anion). The dashed lines show the experimental and simulated anisotropic spectra of three distinct Mg sites. Reproduced with permission.[117] Copyright 2012, American Chemical Society. (b) ^{1}H MAS, ^{1}H{^{27}Al} TRAPDOR NMR spectra along with the ^{1}H signals assignments of deuterated MgAl-25.1 (25.1% of Mg^{2+} is substituted by Al^{3+}). (c) The mole percentages of Mg$_3$OH and Mg$_2$AlOH environments as a function of Al loadings. Reproduced with permission.[118] Copyright 2014, American Chemical Society.

Versatile SSNMR techniques have been applied to extract detailed structural information on various types of LDHs.[119] The dehydration and dehydroxylation processes of LDHs were examined using ^{1}H and ^{27}Al MAS NMR. Dehydration of Mg and Al containing LDHs proceeded below thermal treatment of 150 °C, above which dehydroxylation of Mg$_2$AlOH and Mg$_3$OH species accompanied with the structure changes of LDHs occured.[119d] The local structures of a LDHs containing paramagnetic Ni^{2+} cations have been revealed from ^{1}H, ^{27}Al, and ^{13}C MAS NMR spectroscopy. The intralayer Ni/Al distributions of the LDHs could be determined from the pseudocontact chemical shifts.[119f, g] ^{1}H and ^{71}Ga SSNMR spectroscopy has been employed to reveal the ordering of Ga^{3+} and various proton environments including Mg$_3$OH, Mg$_2$GaOH and water in magnesium gallium (MgGa) LDHs.[119h]

6.2.3 Layered silicates

Layered silicates have attracted broad interests in many applications such as catalysis and adsorption due to their high capacities for ion exchange and easy functionalization by various modifications such as silylation and pillaring. Layered silicates can also serve as precursors for the formation of zeolites by conversion of the 2D frameworks into structurally related 3D porous materials. ^{29}Si, ^{1}H, ^{13}C multi-nuclear SSNMR was frequently utilized to explore the

coordination, stacking geometries, interlayer structures of various layered silicates including RUB-51, HUS-1, PLS-3, PLS-4, HUS-2, HUS-3, HUS-4, and HUS-7. [120] The silicate framework structure of a new layered silicate material named CLS-1 was effectively solved using state-of-the-art NMR crystallography technique (2D ^{29}Si DQ-SQ MAS NMR jointed with XRD and DFT calculations). [121] Recently, the possible crystal structure of magadiite as one of representative layered silicates has been determined using X-ray pair distribution functions and synchrotron powder diffractometry. [122] A combination of diffraction technique, SSNMR and DFT theoretical calculation would provide promising opportunities to extract long- and short-range structural constraints and enable determination of the molecular structure of the layered silicates in the presence of various extents of stacking disorder.

7. Conclusion and outlook

From inorganic to inorganic-organic hybrid and organic framework and from 2D layers to 3D architecture, the microporous materials undergo enormous development. The increasing application of these materials is fuelled by the interest in taking advantage of their diverse structure and properties. The in-depth characterization of the microporous materials at atomic-level plays a critical role for a better understanding of their functions that could lead to new applications.

The structural and chemical complexity involved in the porous materials is beyond the use of some characterization techniques. Multidimensional and multinuclear SSNMR spectroscopy has been successfully used to investigate several representative porous materials including zeolites, MOFs, COFs, PAFs, and layered materials. Due to the advancement in experimental method and hardware, SSNMR has provided detailed information on the local structures, dynamic behaviors of molecules, and host-guest interactions in these porous materials, which is essential for the establishment of their structure-property relationships and hence, the rational design of new functional porous materials.

Although the SSNMR characterization has reached a new level, the rapid development of porous materials also brings novel challenges for the application of SSNMR in this exciting field. The heterogeneous distribution of the framework or extra-framework elements in porous materials, paramagnetic components and the nuclei with low natural abundance and/or large very large quadrupolar interactions significantly lower the NMR detection sensitivity and spectral resolution, which limits the application of the SSNMR with available methodologies. Additionally, obtaining the information at working condition relevant for synthesis, phase change, gas adsorption/separation and catalytic reactions remains one of the most sought after goals in the SSNMR study of porous materials.

Further enhancement in NMR sensitivity is expected from the development of new instrumentation and pulse sequences. For instance, the utility of SSNMR could be significantly improved by using advanced instruments, such as ultra-high field spectrometer equipped with ultra-fast MAS probe. High-resolution SSNMR at magnetic field of 35.2 T is now accessible.[123] The dramatic sensitivity enhancement was demonstrated on ^{17}O [124] and ^{43}Ca spectra[125], which provides opportunities to explore the porous materials with half-integer quadrupolar nuclei at very high field strength. The use of ^{1}H MAS NMR at moderate MAS speed in organic framework porous material is often problematic due to the low spectral resolution caused by strongly coupled ^{1}H–^{1}H spin interactions. The MAS frequency on commercially available probes has reached beyond 110 kHz, the important role of which has been recognized in biochemistry system.[126] The benefit of ultra-fast MAS probe would be demonstrated on porous materials containing paramagnetic ions by reducing the signal broadening caused by paramagnetic shift. DNP technique undoubtedly continues to push the frontiers of SSNMR in material science as it enables sensitivity enhancement larger than two orders of magnitude, which leads to experimental time-saving by four orders of magnitude. The increasing availability of DNP equipment in research community and the introduction of novel experimental protocols (e.g, polarizing agent, solvent and sample preparation) opens

numerous opportunities for its routine use for characterization of porous materials. In situ NMR technique for operando detection is crucial for the investigation of porous materials. Despite the technical challenges, SSNMR probes capable of working under harsh condition such as extremely high/low temperature and high pressure have been built.[58c]

Advanced SSNMR opens new avenue for structural and functional characterization in material science. The combination of NMR spectroscopy with complementary techniques, such as XRD, X-ray adsorption spectroscopy (XAS) and microscopy, would allow the composition and structure of materials to be determined on wide range of length scale and in different dimensions. The obtained atomic-level insights will benefit materials properties improvement and new material discovery.

Acknowledgements

References

[1] a) D. H. Brouwer, M. Horvath, Solid State Nucl. Magn. Reson. 2015, 65, 89; b) F. Taulelle, B. Bouchevreau, C. Martineau, CrystEngComm 2013, 15, 8613; c) S. E. Ashbrook, D. M. Dawson, V. R. Seymour, Phys. Chem. Chem. Phys. 2014, 16, 8223.

[2] a) B. F. Chmelka, J. Magn. Reson. 2019, 306, 91; b) G. Paul, C. Bisio, I. Braschi, M. Cossi, G. Gatti, E. Gianotti, L. Marchese, Chem. Soc. Rev. 2018, 47, 5684; c) V. J. Witherspoon, J. Xu, J. A. Reimer, Chem. Rev. 2018, 118, 10033; d) M. Hunger, W. Wang,

Adv. Catal., 2006, 50, 149; e) B. E. G. Lucier, S. S. Chen, Y. N. Huang, Acc. Chem. Res. 2018, 51, 319; f) J. Xu, Q. Wang, F. Deng, Acc. Chem. Res. 2019, 52, 2179; g) S. Li, F. Deng, Annu. Rep. NMR Spectrosc., 2013, 78, 1; h) *NMR techniques in catalysis*, A. T. Bell, A. Pines (Eds.), Marcel Dekker Inc, New York, 1994; i) *Solid-State NMR Spectroscopy of Inorganic Materials*, J. J. Fitzgerald (Ed.), Oxford University Press, USA 1999; j) G. Engelhardt, D. Michel, *High-Resolution Solid-State NMR of Silicates and Zeolites*, Wiley, New York, 1987; k) J. Xu, Q. Wang, S. Li, F. Deng, *Solid-State NMR in Zeolite Catalysis*, Springer, Singapore, 2019.

[3] a) S. T. Xu, W. P. Zhang, X. C. Liu, X. W. Han, X. H. Bao, J. Am. Chem. Soc. 2009, 131, 13722; b) H. C. Hoffmann, B. Assfour, F. Epperlein, N. Klein, S. Paasch, I. Senkovska, S. Kaskel, G. Seifert, E. Brunner, J. Am. Chem. Soc. 2011, 133, 8681; c) E. Weiland, M. A. Springuel-Huet, A. Nossov, A. Gedeon, Micropor. Mesopor. Mater. 2016, 225, 41; d) S. Komulainen, J. Roukala, V. V. Zhivonitko, M. A. Javed, L. J. Chen, D. Holden, T. Hasell, A. Cooper, P. Lantto, V. V. Telkki, Chem. Sci. 2017, 8, 5721.

[4] a) S. Bureekaew, S. Horike, M. Higuchi, M. Mizuno, T. Kawamura, D. Tanaka, N. Yanai, S. Kitagawa, Nat. Mater. 2009, 8, 831; b) N. B. Shustova, T. C. Ong, A. F. Cozzolino, V. K. Michaelis, R. G. Griffin, M. Dinca, J. Am. Chem. Soc. 2012, 134, 15061; c) A. Comotti, S. Bracco, P. Sozzani, Acc. Chem. Res. 2016, 49, 1701; d) Y. Yan, D. I. Kolokolov, I. da Silva, A. G. Stepanov, A. J. Blake, A. Dailly, P. Manuel, C. C. Tang, S. Yang, M. Schröder, J. Am. Chem. Soc. 2017, 139, 13349.

[5] a) Y. T. A. Wong, V. Martins, B. E. G. Lucier, Y. N. Huang, Chem. - Eur. J. 2019, 25, 1848; b) E. Brunner, M. Rauche, Chem. Sci. 2020, 11, 4297; c) A. Marchetti, J. E. Chen, Z. F. Pang, S. H. Li, D. S. Ling, F. Deng, X. Q. Kong, Adv. Mater. 2017, 29, 1605895.

[6] X. Kong, E. Scott, W. Ding, J. A. Mason, J. R. Long, J. A. Reimer, J. Am. Chem. Soc. 2012, 134, 14341.

[7] A. Medek, J. S. Harwood, L. Frydman, J. Am. Chem. Soc. 1995, 117, 12779.

[8] A. P. M. Kentgens, D. Iuga, M. Kalwei, H. Koller, J. Am. Chem. Soc. 2001, 123, 2925.

[9] a) D. H. Brouwer, P. E. Kristiansen, C. A. Fyfe, M. H. Levitt, J. Am. Chem. Soc. 2005, 127, 542; b) D. H. Brouwer, R. J. Darton, R. E. Morris, M. H. Levitt, J. Am. Chem. Soc. 2005, 127, 10365; c) M. Goswami, P. K. Madhu, J. Dittmer, N. C. Nielsen, S. Ganapathy, Chem. Phys. Lett. 2009, 478, 287.

[10] a) D. F. Shantz, J. Gunne, H. Koller, R. F. Lobo, J. Am. Chem. Soc. 2000, 122, 6659; b) S. Li, A. Zheng, Y. Su, H. Zhang, L. Chen, J. Yang, C. Ye, F. Deng, J. Am. Chem. Soc. 2007, 129, 11161; c) S. Devautour-Vinot, G. Maurin, C. Serre, P. Horcajada, D. P. da Cunha, V. Guillerm, E. D. Costa, F. Taulelle, C. Martineau, Chem. Mater. 2012, 24, 2168.

[11] S. Cadars, D. H. Brouwer, B. F. Chmelka, Phys. Chem. Chem. Phys. 2009, 11, 1825.

[12] a) Z. Yu, A. Zheng, Q. Wang, L. Chen, J. Xu, J. P. Amoureux, F. Deng, Angew. Chem., Int. Ed. 2010, 49, 8657; b) N. Malicki, G. Mali, A.-A. Quoineaud, P. Bourges, L. J. Simon, F. Thibault-Starzyk, C. Fernandez, Micropor. Mesopor. Mater. 2010, 129, 100.

[13] a) D. Massiot, F. Fayon, B. Alonso, J. Trebosc, J. P. Amoureux, J. Magn. Reson. 2003, 164, 160; b) M. N. Garaga, M.-F. Hsieh, Z. Nour, M. Deschamps, D. Massiot, B. F. Chmelka, S. Cadars, Phys. Chem. Chem. Phys. 2015, 17, 21664; c) Z. J. Berkson, M.-F. Hsieh, S. Smeets, D. Gajan, A. Lund, A. Lesage, D. Xie, S. I. Zones, L. B. McCusker, C. Baerlocher, B. F. Chmelka, Angew. Chem., Int. Ed. 2019, 58, 6255.

[14] T. Gullion, J. Schaefer, J. Magn. Reson. 1989, 81, 196.

[15] C. P. Grey, W. S. Veeman, Chem. Phys. Lett. 1992, 192, 379.

[16] T. Gullion, Chem. Phys. Lett. 1995, 246, 325.

[17] a) L. Chen, Q. Wang, B. Hu, O. Lafon, J. Trébosc, F. Deng, J. P. Amoureux, Phys. Chem. Chem. Phys. 2010, 12, 9395; b) S. Li, F. Pourpoint, J. Trébosc, L. Zhou, O. Lafon, M. Shen, A. Zheng, Q. Wang, J.-P. Amoureux, F. Deng, J. Phys. Chem. Lett. 2014, 5, 3068.

[18] F. Pourpoint, A. S. L. Thankamony, C. Volkringer, T. Loiseau, J. Trebosc, F. Aussenac, D. Carnevale, G. Bodenhausen, H. Vezin, O. Lafon, J. P. Amoureux, Chem. Commun. 2014, 50,

933.

[19] K. Chen, S. Horstmeier, V. T. Nguyen, B. Wang, S. P. Crossley, T. Pham, Z. Gan, I. Hung, J. L. White, J. Am. Chem. Soc. 2020, 142, 7514.

[20] a) J. Xu, V. V. Terskikh, Y. Huang, Chem. - Eur. J. 2013, 19, 4432; b) A. Sutrisno, V. V. Terskikh, Q. Shi, Z. W. Song, J. X. Dong, S. Y. Ding, W. Wang, B. R. Provost, T. D. Daff, T. K. Woo, Y. N. Huang, Chem. - Eur. J. 2012, 18, 12251.

[21] a) P. He, B. E. G. Lucier, V. V. Terskikh, Q. Shi, J. Dong, Y. Chu, A. Zheng, A. Sutrisno, Y. Huang, J. Phys. Chem. C 2014, 118, 23728; b) G. D. Qi, Q. Wang, J. Xu, J. Trebosc, O. Lafon, C. Wang, J. P. Amoureux, F. Deng, Angew. Chem., Int. Ed. 2016, 55, 15826.

[22] a) W. R. Gunther, V. K. Michaelis, M. A. Caporini, R. G. Griffin, Y. Roman-Leshkov, J. Am. Chem. Soc. 2014, 136, 6219; b) P. Wolf, M. Valla, A. J. Rossini, A. Comas-Vives, F. Nunez-Zarur, B. Malaman, A. Lesage, L. Emsley, C. Coperet, I. Hermans, Angew. Chem., Int. Ed. 2014, 53, 10179.

[23] T. Kobayashi, F. A. Perras, T. W. Goh, T. L. Metz, W. Huang, M. Pruski, J. Phys. Chem. Lett. 2016, 7, 2322.

[24] A. D. Chowdhury, I. Yarulina, E. Abou-Hamad, A. Gurinov, J. Gascon, Chem. Sci. 2019, 10, 8946.

[25] a) C. A. Fyfe, Y. Feng, H. Grondey, G. T. Kokotailo, H. Gies, Chem. Rev. 1991, 91, 1525; b) J. Klinowski, Chem. Rev. 1991, 91, 1459.

[26] D. H. Brouwer, J. Am. Chem. Soc. 2008, 130, 6306.

[27] R. M. Shayib, N. C. George, R. Seshadri, A. W. Burton, S. I. Zones, B. F. Chmelka, J. Am. Chem. Soc. 2011, 133, 18728.

[28] S. Smeets, Z. J. Berkson, D. Xie, S. I. Zones, W. Wan, X. Zou, M.-F. Hsieh, B. F. Chmelka, L. B. McCusker, C. Baerlocher, J. Am. Chem. Soc. 2017, 139, 16803.

[29] G. P. M. Bignami, D. M. Dawson, V. R. Seymour, P. S. Wheatley, R. E. Morris, S. E. Ashbrook, J. Am. Chem. Soc. 2017, 139, 5140.

[30] C. J. Heard, L. Grajciar, C. M. Rice, S. M. Pugh, P. Nachtigall, S. E. Ashbrook, R. E. Morris, Nat. Commun. 2019, 10, 4690.

[31] a) L. M. Peng, Y. Liu, N. J. Kim, J. E. Readman, C. P. Grey, Nat. Mater. 2005, 4, 216; b) L. Peng, H. Huo, Y. Liu, C. P. Grey, J. Am. Chem. Soc. 2007, 129, 335; c) H. Huo, L. M. Peng, Z. H. Gan, C. P. Grey, J. Am. Chem. Soc. 2012, 134, 9708; d) H. Huo, L. Peng, C. P. Grey, J. Phys. Chem. C 2011, 115, 2030.

[32] a) S. M. Pugh, P. A. Wright, D. J. Law, N. Thompson, S. E. Ashbrook, J. Am. Chem. Soc. 2020, 142, 900; b) B. Chen, Y. Huang, J. Am. Chem. Soc. 2006, 128, 6437.

[33] A. Vjunov, J. L. Fulton, T. Huthwelker, S. Pin, D. Mei, G. K. Schenter, N. Govind, D. M. Camaioni, J. Z. Hu, J. A. Lercher, J. Am. Chem. Soc. 2014, 136, 8296.

[34] a) J. Brus, L. Kobera, W. Schoefberger, M. Urbanova, P. Klein, P. Sazama, E. Tabor, S. Sklenak, A. V. Fishchuk, J. Dedecek, Angew. Chem., Int. Ed. 2015, 54, 541; b) S. Xin, Q. Wang, J. Xu, Y. Chu, P. Wang, N. Feng, G. Qi, J. Trébosc, O. Lafon, W. Fan, F. Deng, Chem. Sci. 2019, 10, 10159.

[35] a) Q. M. Wu, X. Wang, G. D. Qi, Q. Guo, S. X. Pan, X. J. Meng, J. Xu, F. Deng, F. T. Fan, Z. C. Feng, C. Li, S. Maurer, U. Muller, F. S. Xiao, J. Am. Chem. Soc. 2014, 136, 4019; b) Q. M. Wu, X. L. Liu, L. F. Zhu, L. H. Ding, P. Gao, X. Wang, S. X. Pan, C. Q. Bian, X. J. Meng, J. Xu, F. Deng, S. Maurer, U. Muller, F. S. Xiao, J. Am. Chem. Soc. 2015, 137, 1052.

[36] Q. M. Wu, L. F. Zhu, Y. Y. Chu, X. L. Liu, C. S. Zhang, J. Zhang, H. Xu, J. Xu, F. Deng, Z. C. Feng, X. J. Meng, F. S. Xiao, Angew. Chem., Int. Ed. 2019, 58, 12138.

[37] Y. Y. Jin, Q. Sun, G. D. Qi, C. G. Yang, J. Xu, F. Chen, X. J. Meng, F. Deng, F. S. Xiao, Angew. Chem., Int. Ed. 2013, 52, 9172.

[38] a) N. Sheng, Y. Y. Chu, S. H. Xing, Q. Wang, X. F. Yi, Z. C. Feng, X. J. Meng, X. L. Liu, F. Deng, F. S. Xiao, J. Am. Chem. Soc. 2016, 138, 6171; b) J. Xu, L. Chen, D. Zeng, J. Yang, M. Zhang, C. Ye, F. Deng, J. Phys. Chem. B 2007, 111, 7105.

[39] G. D. Qi, Q. Wang, J. Xu, Q. M. Wu, C. Wang, X. L. Zhao, X. J. Meng, F. S. Xiao, F.

Deng, Commun. Chem. 2018, 1, 22.

[40] a) H. Zheng, D. Ma, X. H. Bao, J. Z. Hu, J. H. Kwak, Y. Wang, C. H. F. Peden, J. Am. Chem. Soc. 2008, 130, 3722; b) J. Z. Hu, J. H. Kwak, Y. Wang, C. H. F. Peden, H. Zheng, D. Ma, X. Bao, J. Phys. Chem. C 2009, 113, 2936.

[41] M. Hunger, Solid State Nucl. Magn. Reson. 1996, 6, 1.

[42] P. Gao, Q. Wang, J. Xu, G. D. Qi, C. Wang, X. Zhou, X. L. Zhou, N. D. Feng, X. L. Liu, F. Deng, ACS Catal. 2018, 8, 69.

[43] Z. Wang, L. A. O'Dell, X. Zeng, C. Liu, S. Zhao, W. Zhang, M. Gaborieau, Y. Jiang, J. Huang, Angew. Chem., Int. Ed. 2019, 58, 18061.

[44] N. Popovych, P. Kyriienko, S. Soloviev, R. Baran, Y. Millot, S. Dzwigaj, Phys. Chem. Chem. Phys. 2016, 18, 29458.

[45] P. Cruz, M. Fajardo, I. del Hierro, Y. Perez, Catal. Sci. Technol. 2019, 9, 620.

[46] a) A. Lopez, M. H. Tuilier, J. L. Guth, L. Delmotte, J. M. Popa, J. Solid State Chem. 1993, 102, 480; b) S. Ganapathy, K. U. Gore, R. Kumar, J. P. Amoureux, Solid State Nucl. Magn. Reson. 2003, 24, 184.

[47] Z. Zhao, W. Zhang, P. Ren, X. Han, U. Müller, B. Yilmaz, M. Feyen, H. Gies, F.-S. Xiao, D. De Vos, T. Tatsumi, X. Bao, Chem. Mater. 2013, 25, 840.

[48] L. Xu, X. Y. Ji, S. H. Li, Z. Y. Zhou, X. Du, J. L. Sun, F. Deng, S. N. Che, P. Wu, Chem. Mater. 2016, 28, 4512.

[49] J. Martinez-Ortigosa, J. Simancas, J. A. Vidal-Moya, P. Gaveau, F. Rey, B. Alonso, T. Blasco, J. Phys. Chem. C 2019, 123, 22324.

[50] M. Kumar, Z. J. Berkson, R. J. Clark, Y. Shen, N. A. Prisco, Q. Zheng, Z. Zeng, H. Zheng, L. B. McCusker, J. C. Palmer, B. F. Chmelka, J. D. Rimer, J. Am. Chem. Soc. 2019, 141, 20155.

[51] a) K. Na, C. Jo, J. Kim, K. Cho, J. Jung, Y. Seo, R. J. Messinger, B. F. Chmelka, R. Ryoo, Science 2011, 333, 328; b) R. J. Messinger, K. Na, Y. Seo, R. Ryoo, B. F. Chmelka, Angew.

Chem., Int. Ed. 2015, 54, 927; c) D. H. Brouwer, S. Cadars, J. Eckert, Z. Liu, O. Terasaki, B. F. Chmelka, J. Am. Chem. Soc. 2013, 135, 5641.

[52] G. Brunklaus, H. Koller, S. I. Zones, Angew. Chem., Int. Ed. 2016, 55, 14459.

[53] A. Corma, H. Garcia, Eur. J. Inorg. Chem. 2004, 2004, 1143.

[54] C. Wang, Q. Wang, J. Xu, G. D. Qi, P. Gao, W. Y. Wang, Y. Y. Zou, N. D. Feng, X. L. Liu, F. Deng, Angew. Chem., Int. Ed. 2016, 55, 2507.

[55] C. Wang, J. Xu, Q. Wang, X. Zhou, G. D. Qi, N. D. Feng, X. L. Liu, X. J. Meng, F. S. Xiao, F. Deng, ACS Catal. 2017, 7, 6094.

[56] C. Wang, Y. Chu, J. Xu, Q. Wang, G. Qi, P. Gao, X. Zhou, F. Deng, Angew. Chem., Int. Ed. 2018, 57, 10197.

[57] D. Xiao, S. T. Xu, X. W. Han, X. E. Bao, Z. M. Liu, F. Blanc, Chem. Sci. 2017, 8, 8309.

[58] a) M. Hunger, J. Weitkamp, Angew. Chem., Int. Ed. 2001, 40, 2954; b) J. F. Haw, W. G. Song, D. M. Marcus, J. B. Nicholas, Acc. Chem. Res. 2003, 36, 317; c) N. R. Jaegers, K. T. Mueller, Y. Wang, J. Z. Hu, Acc. Chem. Res. 2020, 53, 611; d) X. Wang, G. Qi, J. Xu, B. Li, C. Wang, F. Deng, Angew. Chem., Int. Ed. 2012, 51, 3850.

[59] a) J.-F. Wu, S.-M. Yu, W. D. Wang, Y.-X. Fan, S. Bai, C.-W. Zhang, Q. Gao, J. Huang, W. Wang, J. Am. Chem. Soc. 2013, 135, 13567; b) W. L. Dai, C. M. Wang, X. F. Yi, A. M. Zheng, L. D. Li, G. J. Wu, N. J. Guan, Z. K. Xie, M. Dyballa, M. Hunger, Angew. Chem., Int. Ed. 2015, 54, 8783; c) S. Xu, A. Zheng, Y. Wei, J. Chen, J. Li, Y. Chu, M. Zhang, Q. Wang, Y. Zhou, J. Wang, F. Deng, Z. Liu, Angew. Chem., Int. Ed. 2013, 52, 11564; d) C. Wang, Y. Chu, A. Zheng, J. Xu, Q. Wang, P. Gao, G. Qi, Y. Gong, F. Deng, Chem. Eur. J. 2014, 20, 12432; e) C. Wang, X. Yi, J. Xu, G. Qi, P. Gao, W. Wang, Y. Chu, Q. Wang, N. Feng, X. Liu, A. Zheng, F. Deng, Chem. - Eur. J. 2015, 21, 12061.

[60] a) X. Wu, S. Xu, W. Zhang, J. Huang, J. Li, B. Yu, Y. Wei, Z. Liu, Angew. Chem., Int. Ed. 2017, 56, 9039; b) X. Zhou, C. Wang, Y. Y. Chu, J. Xu, Q. Wang, G. D. Qi, X. L. Zhao, N. D. Feng, F. Deng, Nat. Commun. 2019, 10, 1961; c) Z. Zhao, H. Shi, C. Wan, M. Y. Hu, Y. Liu,

D. Mei, D. M. Camaioni, J. Z. Hu, J. A. Lercher, J. Am. Chem. Soc. 2017, 139, 9178.

[61] H. Furukawa, K. E. Cordova, M. O'Keeffe, O. M. Yaghi, Science 2013, 341, 974.

[62] R. S. K. Madsen, A. Qiao, J. Sen, I. Hung, K. Chen, Z. Gan, S. Sen, Y. Yue, Science 2020, 367, 1473.

[63] S. S. Chen, B. E. G. Lucier, M. S. Chen, V. V. Terskikh, Y. N. Huang, Chem. Eur. J. 2018, 24, 8732.

[64] Y. Zhang, B. E. G. Lucier, V. V. Terskikh, R. L. Zheng, Y. N. Huang, Solid State Nucl. Magn. Reson. 2017, 84, 118.

[65] Y. Jiang, J. Huang, S. Marx, W. Kleist, M. Hunger, A. Baiker, J. Phys. Chem. Lett. 2010, 1, 2886.

[66] P. He, J. Xu, V. V. Terskikh, A. Sutrisno, H.-Y. Nie, Y. Huang, J. Phys. Chem. C 2013, 117, 16953.

[67] G. P. M. Bignami, Z. H. Davis, D. M. Dawson, S. A. Morris, S. E. Russell, D. McKay, R. E. Parke, D. Iuga, R. E. Morris, S. E. Ashbrook, Chem. Sci. 2018, 9, 850.

[68] a) J. Xu, V. V. Terskikh, Y. Chu, A. Zheng, Y. Huang, Chem. Mater. 2015, 27, 3306; b) D. M. Dawson, L. E. Jamieson, M. I. H. Mohideen, A. C. McKinlay, I. A. Smellie, R. Cadou, N. S. Keddie, R. E. Morris, S. E. Ashbrook, Phys. Chem. Chem. Phys. 2013, 15, 919; c) T. Wittmann, A. Mondal, C. B. L. Tschense, J. J. Wittmann, O. Klimm, R. Siegel, B. Corzilius, B. Weber, M. Kaupp, J. Senker, J. Am. Chem. Soc. 2018, 140, 2135; d) E. F. Baxter, T. D. Bennett, C. Mellot-Draznieks, C. Gervais, F. Blanc, A. K. Cheetham, Phys. Chem. Chem. Phys. 2015, 17, 25191; e) S. Sneddon, J. Kahr, A. F. Orsi, D. J. Price, D. M. Dawson, P. A. Wright, S. E. Ashbrook, Solid State Nucl. Magn. Reson. 2017, 87, 54.

[69] J. T. Damron, J. L. Ma, R. Kurz, K. Saalwaechter, A. J. Matzger, A. Ramamoorthy, Angew. Chem., Int. Ed. 2018, 57, 8678.

[70] a) M. Inukai, M. Tamura, S. Horike, M. Higuchi, S. Kitagawa, K. Nakamura, Angew. Chem., Int. Ed. 2018, 57, 8687; b) A. Gonzalez-Nelson, F. X. Coudert, M. A. van der Veen,

Nanomaterials 2019, 9, 330.

[71] H. Deng, C. J. Doonan, H. Furukawa, R. B. Ferreira, J. Towne, C. B. Knobler, B. Wang, O. M. Yaghi, Science 2010, 327, 846.

[72] X. Kong, H. Deng, F. Yan, J. Kim, J. A. Swisher, B. Smit, O. M. Yaghi, J. A. Reimer, Science 2013, 341, 882.

[73] A. Krajnc, T. Kos, N. Z. Logar, G. Mali, Angew. Chem., Int. Ed. 2015, 54, 10535.

[74] A. Krajnc, B. Bueken, D. De Vos, G. Mali, J. Magn. Reson. 2017, 279, 22.

[75] a) K. C. Jayachandrababu, R. J. Verploegh, J. Leisen, R. C. Nieuwendaal, D. S. Sholl, S. Nair, J. Am. Chem. Soc. 2016, 138, 7325; b) K. C. Jayachandrababu, D. S. Sholl, S. Nair, J. Am. Chem. Soc. 2017, 139, 5906.

[76] B. E. G. Lucier, Y. Zhang, K. J. Lee, Y. Lu, Y. Huang, Chem. Commun. 2016, 52, 7541.

[77] Y. Zhang, B. E. G. Lucier, M. Fischer, Z. Gan, P. D. Boyle, B. Desveaux, Y. Huang, Chem. - Eur. J. 2018, 24, 7866.

[78] S. Chen, S. Mukherjee, B. E. G. Lucier, Y. Guo, Y. T. A. Wong, V. V. Terskikh, M. J. Zaworotko, Y. Huang, J. Am. Chem. Soc. 2019, 141, 14257.

[79] a) J. Li, S. Li, A. Zheng, X. Liu, N. Yu, F. Deng, J. Phys. Chem. C 2017, 121, 14261; b) Y. Xiao, Y. Chu, S. Li, Y. Su, J. Tang, J. Xu, F. Deng, J. Phys. Chem. C 2020, 124, 3738.

[80] V. J. Witherspoon, R. Mercado, E. Braun, A. Mace, J. Bachman, J. R. Long, B. Blümich, B. Smit, J. A. Reimer, J. Phys. Chem. C 2019, 123, 12286.

[81] a) Y. Zhang, B. E. G. Lucier, S. M. McKenzie, M. Arhangelskis, A. J. Morris, T. Friscic, J. W. Reid, V. V. Terskikh, M. Chen, Y. Huang, ACS Appl. Mater. Inter. 2018, 10, 28582; b) Y. Zhang, B. E. G. Lucier, Y. Huang, Phys. Chem. Chem. Phys. 2016, 18, 8327; c) W. D. Wang, B. E. G. Lucier, V. V. Terskikh, W. Wang, Y. Huang, J. Phys. Chem. Lett. 2014, 5, 3360; d) Y. Lu, B. E. G. Lucier, Y. Zhang, P. Ren, A. Zheng, Y. Huang, Phys. Chem. Chem. Phys. 2017, 19, 6130; e) B. E. Desveaux, Y. T. A. Wong, B. E. G. Lucier, V. V. Terskikh, P. D. Boyle, S. Jiang, Y. Huang, J. Phys. Chem. C 2019, 123, 17798; f) S. Chen, B. E. G. Lucier, P. D. Boyle,

Y. Huang, Chem. Mater. 2016, 28, 5829.

[82] T. M. McDonald, J. A. Mason, X. Q. Kong, E. D. Bloch, D. Gygi, A. Dani, V. Crocella, F. Giordanino, S. O. Odoh, W. S. Drisdell, B. Vlaisavljevich, A. L. Dzubak, R. Poloni, S. K. Schnell, N. Planas, K. Lee, T. Pascal, L. W. F. Wan, D. Prendergast, J. B. Neaton, B. Smit, J. B. Kortright, L. Gagliardi, S. Bordiga, J. A. Reimer, J. R. Long, Nature 2015, 519, 303.

[83] A. C. Forse, P. J. Milner, J. H. Lee, H. N. Redfearn, J. Oktawiec, R. L. Siegelman, J. D. Martell, B. Dinakar, L. B. Porter-Zasada, M. I. Gonzalez, J. B. Neaton, J. R. Long, J. A. Reimer, J. Am. Chem. Soc. 2018, 140, 18016.

[84] A. C. Forse, M. I. Gonzalez, R. L. Siegelman, V. J. Witherspoon, S. Jawahery, R. Mercado, P. J. Milner, J. D. Martell, B. Smit, B. Blümich, J. R. Long, J. A. Reimer, J. Am. Chem. Soc. 2018, 140, 1663.

[85] a) R. L. Siegelman, P. J. Milner, A. C. Forse, J.-H. Lee, K. A. Colwell, J. B. Neaton, J. A. Reimer, S. C. Weston, J. R. Long, J. Am. Chem. Soc. 2019, 141, 13171; b) P. J. Milner, R. L. Siegelman, A. C. Forse, M. I. Gonzalez, T. Runcevski, J. D. Martell, J. A. Reimer, J. R. Long, J. Am. Chem. Soc. 2017, 139, 13541.

[86] V. Y. Mao, P. J. Milner, J.-H. Lee, A. C. Forse, E. J. Kim, R. L. Siegelman, C. M. McGuirk, L. B. Porter-Zasada, J. B. Neaton, J. A. Reimer, J. R. Long, Angew. Chem., Int. Ed. 2020, 59, 10.1002/anie.201915561.

[87] S.-Y. Ding, W. Wang, Chem. Soc. Rev. 2013, 42, 548.

[88] a) A. Acharjya, P. Pachfule, J. Roeser, F.-J. Schmitt, A. Thomas, Angew. Chem., Int. Ed. 2019, 58, 14865; b) S. Chandra, S. Kandambeth, B. P. Biswal, B. Lukose, S. M. Kunjir, M. Chaudhary, R. Babarao, T. Heine, R. Banerjee, J. Am. Chem. Soc. 2013, 135, 17853; c) P. J. Waller, S. J. Lyle, T. M. O. Popp, C. S. Diercks, J. A. Reimer, O. M. Yaghi, J. Am. Chem. Soc. 2016, 138, 15519; d) J. X. Ma, J. Li, Y.-F. Chen, R. Ning, Y.-F. Ao, J.-M. Liu, J. Sun, D.-X. Wang, Q. Q. Wang, J. Am. Chem. Soc. 2019, 141, 3843; e) H. Lyu, C. S. Diercks, C. Zhu, O. M. Yaghi, J. Am. Chem. Soc. 2019, 141, 6848; f) E. Troschke, S. Graetz, T. Luebken, L.

Borchardt, Angew. Chem., Int. Ed. 2017, 56, 6859; g) Y. Zhi, P. Shao, X. Feng, H. Xia, Y. Zhang, Z. Shi, Y. Mu, X. Liu, J. Mater. Chem. A 2018, 6, 374; h) T. Ma, E. A. Kapustin, S. X. Yin, L. Liang, Z. Zhou, J. Niu, L. H. Li, Y. Wang, J. Su, J. Li, X. Wang, W. D. Wang, W. Wang, J. Sun, O. M. Yaghi, Science 2018, 361, 48.

[89] a) K. Gottschling, L. Stegbauer, G. Sayasci, N. A. Prisco, Z. J. Berkson, C. Ochsenfeld, B. F. Chmelka, B. V. Lotsch, Chem. Mater. 2019, 31, 1946; b) S. J. Lyle, T. M. O. Popp, P. J. Waller, X. Pei, J. A. Reimer, O. M. Yaghi, J. Am. Chem. Soc. 2019, 141, 11253; c) P. Tomaszewski, M. Wiszniewski, K. Gontarczyk, P. Wiecinski, K. Durka, S. Lulinski, Polymers 2019, 11, 1070; d) Y.-X. Ma, Z.-J. Li, L. Wei, S. Y. Ding, Y. B. Zhang, W. Wang, J. Am. Chem. Soc. 2017, 139, 4995.

[90] Y. Du, H. Yang, J. M. Whiteley, S. Wan, Y. Jin, S.-H. Lee, W. Zhang, Angew. Chem., Int. Ed. 2016, 55, 1737.

[91] W. Cao, W. D. Wang, H.-S. Xu, I. V. Sergeyev, J. Struppe, X. Wang, F. Mentink-Vigier, Z. Gan, M.-X. Xiao, L.-Y. Wang, G.-P. Chen, S.-Y. Ding, S. Bai, W. Wang, J. Am. Chem. Soc. 2018, 140, 6969.

[92] S. Y. Ding, M. Dong, Y.-W. Wang, Y. T. Chen, H. Z. Wang, C. Y. Su, W. Wang, J. Am. Chem. Soc. 2016, 138, 3031.

[93] G. Zhang, Y. L. Hong, Y. Nishiyama, S. Bai, S. Kitagawa, S. Horike, J. Am. Chem. Soc. 2019, 141, 1227.

[94] Y. Du, D. Calabro, B. Wooler, Q. Li, S. Cundy, P. Kamakoti, D. Colmyer, K. Mao, P. Ravikovitch, J. Phys. Chem. C 2014, 118, 399.

[95] Y. Du, K. M. Mao, P. Kamakoti, B. Wooler, S. Cundy, Q. C. Li, P. Ravikovitch, D. Calabro, J. Mater. Chem. A 2013, 1, 13171.

[96] a) L. Jiao, Y. Wang, H. L. Jiang, Q. Xu, Adv. Mater. 2018, 30, 1703663; b) S. M. J. Rogge, A. Bavykina, J. Hajek, H. Garcia, A. I. Olivos-Suarez, A. Sepulveda-Escribano, A. Vimont, G. Clet, P. Bazin, F. Kapteijn, M. Daturi, E. V. Ramos-Fernandez, F. Xamena, V. Van

Speybroeck, J. Gascon, Chem. Soc. Rev. 2017, 46, 3134; c) Q. H. Yang, Q. Xu, H. L. Jiang, Chem. Soc. Rev. 2017, 46, 4774; d) L. Zhu, X. Q. Liu, H. L. Jiang, L. B. Sun, Chem. Rev. 2017, 117, 8129.

[97] a) J. C. Jiang, F. Gandara, Y. B. Zhang, K. Na, O. M. Yaghi, W. G. Klemperer, J. Am. Chem. Soc. 2014, 136, 12844; b) C. A. Trickett, T. M. O. Popp, J. Su, C. Yan, J. Weisberg, A. Huq, P. Urban, J. C. Jiang, M. J. Kalmutzki, Q. N. Liu, J. Baek, M. P. Head-Gordon, G. A. Somorjai, J. A. Reimer, O. M. Yaghi, Nat. Chem. 2019, 11, 170; c) M. D. de Mello, G. Kumar, T. Tabassum, S. K. Jain, T. H. Chen, S. Caratzoulas, X. Y. Li, D. G. Vlachos, S. I. Han, S. L. Scott, P. Dauenhauer, M. Tsapatsis, Angew. Chem., Int. Ed. 2020, 59, 10.1002/anie.202001332 ; d) W. K. An, M. Y. Han, C. A. Wang, S. M. Yu, Y. Zhang, S. Bai, W. Wang, Chem. - Eur. J. 2014, 20, 11019; e) Y. Z. Chen, B. C. Gu, T. Uchida, J. D. Liu, X. C. Liu, B. J. Ye, Q. Xu, H. L. Jiang, Nat. Commun. 2019, 10, 3462.

[98] Y. Tian, G. Zhu, Chem. Rev. 2020, 120, 10.1021/acs.chemrev.9b00687.

[99] T. Ben, H. Ren, S. Ma, D. Cao, J. Lan, X. Jing, W. Wang, J. Xu, F. Deng, J. M. Simmons, S. Qiu, G. Zhu, Angew. Chem., Int. Ed. 2009, 48, 9457.

[100] H. Ren, T. Ben, F. Sun, M. Guo, X. Jing, H. Ma, K. Cai, S. Qiu, G. Zhu, J. Mater. Chem. 2011, 21, 10348.

[101] T. Ben, K. Shi, Y. Cui, C. Pei, Y. Zuo, H. Guo, D. Zhang, J. Xu, F. Deng, Z. Tian, S. Qiu, J. Mater. Chem. 2011, 21, 18208.

[102] B. Liu, T. Ben, J. Xu, F. Deng, S. Qiu, New J. Chem. 2014, 38, 2292.

[103] M. Errahali, G. Gatti, L. Tei, G. Paul, G. A. Rolla, L. Canti, A. Fraccarollo, M. Cossi, A. Comotti, P. Sozzani, L. Marchese, J. Phys. Chem. C 2014, 118, 28699.

[104] M. G. Goesten, A. Szecsenyi, M. F. de Lange, A. V. Bavykina, K. B. S. S. Gupta, F. Kapteijn, J. Gascon, ChemCatChem 2016, 8, 961.

[105] S. Bracco, D. Piga, I. Bassanetti, J. Perego, A. Comotti, P. Sozzani, J. Mater. Chem. A 2017, 5, 10328.

[106] Y. Peng, T. Ben, J. Xu, M. Xue, X. Jing, F. Deng, S. Qiu, G. Zhu, Dalton Trans. 2011, 40, 2720.

[107] T. Ben, C. Pei, D. Zhang, J. Xu, F. Deng, X. Jing, S. Qiu, Energy Environ. Sci. 2011, 4, 3991.

[108] M. Li, H. Ren, F. Sun, Y. Tian, Y. Zhu, J. Li, X. Mu, J. Xu, F. Deng, G. Zhu, Adv. Mater. 2018, 30, 1804169.

[109] A. Comotti, S. Bracco, T. Ben, S. Qiu, P. Sozzani, Angew. Chem., Int. Ed. 2014, 53, 1043.

[110] B. Xu, J. Leisen, H. W. Beckham, R. Abu-Zurayk, E. Harkin-Jones, T. McNally, Macromolecules 2009, 42, 8959.

[111] X. J. Ai, L. Chen, J. X. Dong, C. H. Ye, F. Deng, J. Mater. Chem. 2003, 13, 614.

[112] C. Zhong, Y. D. Deng, W. B. Hu, J. L. Qiao, L. Zhang, J. J. Zhang, Chem. Soc. Rev. 2015, 44, 7484.

[113] H. Banda, S. Perie, B. Daffos, P.-L. Taberna, L. Dubois, O. Crosnier, P. Simon, D. Lee, G. De Paepe, F. Duclairoir, ACS Nano 2019, 13, 1443.

[114] J. Cai, J. Chen, P. Zeng, Z. Pang, X. Kong, Chem. Mater. 2019, 31, 3729.

[115] a) R. Liu, G. Zhang, H. Cao, S. Zhang, Y. Xie, A. Haider, U. Kortz, B. Chen, N. S. Dalal, Y. Zhao, L. Zhi, C.-X. Wu, L.-K. Yan, Z. Su, B. Keita, Energy Environ. Sci. 2016, 9, 1012; b) I. A. Vacchi, C. Spinato, J. Raya, A. Bianco, C. Menard-Moyon, Nanoscale 2016, 8, 13714; c) M. Leskes, G. Kim, T. Liu, A. L. Michan, F. Aussenac, P. Dorffer, S. Paul, C. P. Grey, J. Phys. Chem. Lett. 2017, 8, 1078; d) K. Li, Z. Bo, J. Yan, K. Cen, Sci. Rep. 2016, 6, 39689; e) A. R. MacIntosh, K. J. Harris, G. R. Goward, Chem. Mater. 2016, 28, 360; f) R. Das, R. Ranjan, N. Sinha, A. M. Kayastha, J. Phys. Chem. C 2018, 122, 19259.

[116] Q. Wang, D. O'Hare, Chem. Rev. 2012, 112, 4124.

[117] P. J. Sideris, F. Blanc, Z. H. Gan, C. P. Grey, Chem. Mater. 2012, 24, 2449.

[118] G. Y. Yu, M. Shen, M. Wang, L. Shen, W. H. Dong, S. Tang, L. Zhao, Z. Qi, N. H. Xue,

X. F. Guo, W. P. Ding, B. W. Hu, L. M. Peng, J. Phys. Chem. Lett. 2014, 5, 363.

[119] a) A. Vyalikh, D. Massiot, U. Scheler, Solid State Nucl. Magn. Reson. 2009, 36, 19; b) G. Yu, F. Hu, H. Huo, W. Ding, L. Peng, Chem. Phys. Lett. 2018, 706, 47; c) V. R. R. Cunha, P. A. D. Petersen, M. B. Goncalves, H. M. Petrilli, C. Taviot-Gueho, F. Leroux, M. L. A. Temperini, V. R. L. Constantino, Chem. Mater. 2012, 24, 1415; d) G. Yu, Y. Zhou, R. Yang, M. Wang, L. Shen, Y. Li, N. Xue, X. Guo, W. Ding, L. Peng, J. Phys. Chem. C 2015, 119, 12325; e) A. Di Bitetto, E. Andre, C. Carteret, P. Durand, G. Kervern, J. Phys. Chem. C 2017, 121, 7276; f) S. Ishihara, K. Deguchi, H. Sato, M. Takegawa, E. Nii, S. Ohki, K. Hashi, M. Tansho, T. Shimizu, K. Ariga, J. Labuta, P. Sahoo, Y. Yamauchi, J. P. Hill, N. Iyi, R. Sasai, RSC Adv. 2013, 3, 19857; g) N. D. Jensen, C. Forano, S. S. C. Pushparaj, Y. Nishiyama, B. Bekele, U. G. Nielsen, Phys. Chem. Chem. Phys. 2018, 20, 25335; h) L. B. Petersen, A. S. Lipton, V. Zorin, U. G. Nielsen, J. Solid State Chem. 2014, 219, 242; i) N. D. Jensen, M. Bjerring, U. G. Nielsen, Solid State Nucl. Magn. Reson. 2016, 78, 9.

[120] a) Z. Li, B. Marler, H. Gies, Chem. Mater. 2008, 20, 1896; b) T. Ikeda, S. Kayamori, F. Mizukami, J. Mater. Chem. 2009, 19, 5518; c) T. Ikeda, Y. Oumi, K. Honda, T. Sano, K. Momma, F. Izumi, Inorg. Chem. 2011, 50, 2294; d) R. Ishii, T. Ikeda, T. Itoh, T. Ebina, T. Yokoyama, T. Hanaoka, F. Mizukami, J. Mater. Chem. 2006, 16, 4035; e) N. Tsunoji, T. Ikeda, Y. Ide, M. Sadakane, T. Sano, J. Mater. Chem. 2012, 22, 13682; f) N. Tsunoji, T. Ikeda, M. Sadakane, T. Sano, J. Mater. Chem. A 2014, 2, 3372.

[121] S. Cadars, M. Allix, D. H. Brouwer, R. Shayib, M. Suchomel, M. N. Garaga, A. Rakhmatullin, A. W. Burton, S. I. Zones, D. Massiot, B. F. Chmelka, Chem. Mater. 2014, 26, 6994.

[122] Y. Ide, S. Tominaka, H. Kono, R. Ram, A. Machida, N. Tsunoji, Chem. Sci. 2018, 9, 8637.

[123] Z. Gan, I. Hung, X. Wang, J. Paulino, G. Wu, I. M. Litvak, P. L. Gor'kov, W. W. Brey, P. Lendi, J. L. Schiano, M. D. Bird, L. R. Dixon, J. Toth, G. S. Boebinger, T. A. Cross, J. Magn.

Reson. 2017, 284, 125.

[124] a) E. G. Keeler, V. K. Michaelis, M. T. Colvin, I. Hung, P. L. Gor'kov, T. A. Cross, Z. Gan, R. G. Griffin, J. Am. Chem. Soc. 2017, 139, 17953; b) Q. Wang, W. Li, I. Hung, F. Mentink-Vigier, X. Wang, G. Qi, X. Wang, Z. Gan, J. Xu, F. Deng, Nat. Commun. 2020, 11, 3620.

[125] C. Bonhomme, X. Wang, I. Hung, Z. Gan, C. Gervais, C. Sassoye, J. Rimsza, J. Du, M. E. Smith, J. V. Hanna, S. Sarda, P. Gras, C. Combes, D. Laurencin, Chem. Commun. 2018, 54, 9591.

[126] J. P. Demers, V. Chevelkov, A. Lange, Solid State Nucl. Magn. Reson. 2011, 40, 101.

Shenhui Li received his Ph.D. degree from physical chemistry from Wuhan Institute of Physics and Mathematics (WIPM), Chinese Academy of Sciences in 2008. He was appointed as a postdoctoral research fellow at Iowa State University during 2008−2010, a visiting scholar at Univ. Lille during 2013 and joined WIPM since 2010. His current research interest focuses on application of solid-state NMR techniques to MOFs and zeolites.


Jun Xu received his PhD (2007) from Wuhan Institute of Physics and Mathematics (WIPM), Chinese Academy of Sciences. He spent one year as a visiting scholar in Cardiff University, UK. Since 2014, he is a professor at WIPM. His research interests are the application and development of solid-state NMR techniques for heterogeneous catalysts and reaction mechanism with a special focus on the transformation of low carbon molecules on zeolites and related materials.

Feng Deng obtained his PhD (1996) from Wuhan Institute of Physics and Mathematics (WIPM), Chinese Academy of Sciences. After his postdoctoral research (1997−1998) at the department of chemistry, Texas A&M University (with Prof. James F. Haw), he has worked at WIPM as a professor since 1999. His research interests include solid-state NMR methodology and its application to heterogeneous catalysis.

ToC figure
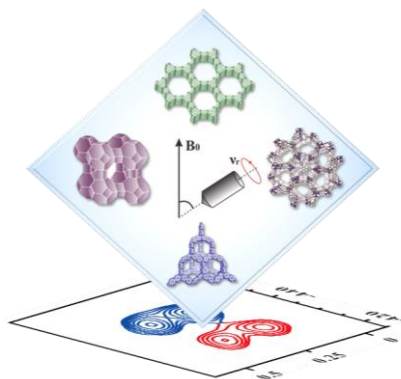
Recent progresses in the application of solid-state NMR in the study of microporous materials are reviewed. The state-of-the-art of solid-state NMR spectroscopies for characterization of structures and dynamics of microporous materials are summarized. The obtained atomic-level information that allows understanding of structure-performance relationships is highlighted.